

# Kilometre-Scale Assessment of the Adriatic Dense Water Multi-Decadal Dynamics

Petra Pranić<sup>1</sup>, Clea Lumina Denamiel<sup>2</sup>, and Ivica Vilibić<sup>2</sup>

<sup>1</sup>Institute of Oceanography and Fisheries

<sup>2</sup>Ruđer Bošković Institute

April 11, 2024

## Abstract

The North Adriatic Dense Water (NAddW) – the densest Mediterranean water generated by extreme cooling during wintertime hurricane-strength winds – drives the thermohaline circulation, ventilates the deep layers, and changes the biogeochemical properties of the Adriatic Sea. However, modelling the dynamical properties of such dense water at the climate scale has been a challenge for decades due to the complex coastal geomorphology of the Adriatic basin not properly reproduced by existing climate models. To overcome these deficiencies, a 31-year-long simulation (1987-2017) of the Adriatic Sea and Coast (AdriSC) kilometre-scale atmosphere-ocean model is used to analyse the main NAddW dynamical phases (i.e., generation, spreading and accumulation). The study highlights four key results. First, during winter, the NAddW densities are higher in the shallow northern Adriatic shelf than in the deeper Kvarner Bay – where 25-35% of the overall NAddW are found to be generated – due to a median bottom temperature difference of 2°C between the two generation sites. Second, the NAddW mass transported across most of the Adriatic peaks between February and May, except along the western side of the Otranto Strait. Third, for the accumulation sites, the bottom layer of the Kvarner Bay is found to be renewed annually while the renewal occurs every 1–3 years in the Jabuka Pit and every 5–10 years in the deep Southern Adriatic Pit. Fourth, the NAddW cascading and accumulation is more pronounced during basin-wide high-salinity conditions driven by circulation changes in the northern Ionian Sea.

## Hosted file

AGU\_Manuscript\_Word\_Apr\_24\_Pranic\_etal.docx available at <https://authorea.com/users/765606/articles/788892-kilometre-scale-assessment-of-the-adriatic-dense-water-multi-decadal-dynamics>

## Hosted file

AGU\_SuppInfo\_Word\_Apr\_24\_Pranic\_etal.docx available at <https://authorea.com/users/765606/articles/788892-kilometre-scale-assessment-of-the-adriatic-dense-water-multi-decadal-dynamics>

1 **Kilometre-Scale Assessment of the Adriatic Dense Water Multi-Decadal Dynamics**

2 **Petra Pranić<sup>1</sup>, Cléa Denamiel<sup>2,3</sup>, and Ivica Vilibić<sup>2,3</sup>**

3 <sup>1</sup>Institute of Oceanography and Fisheries, Šetalište I. Meštrovića 63, 21000 Split, Croatia.

4 <sup>2</sup>Ruder Bošković Institute, Division for Marine and Environmental Research, Bijenička cesta 54,  
5 10000 Zagreb, Croatia.

6 <sup>3</sup>Institute for Adriatic Crops and Karst Reclamation, Put Duilova 11, 21000 Split, Croatia.

7 Corresponding author: Petra Pranić ([pranic@izor.hr](mailto:pranic@izor.hr))

8 **Key Points:**

- 9       • The kilometre-scale dense water generation, spreading and accumulation is quantified in  
10       the Adriatic Sea during the 1987–2017 period
- 11       • About a third of the dense water is generated within the Kvarner Bay which is deeper and  
12       warmer than the well-studied main generation site
- 13       • The bottom layer renewal of the accumulation sites is annual in the Kvarner Bay and up to  
14       decadal in the deepest Adriatic pits

**15 Abstract**

16 The North Adriatic Dense Water (NAddW) – the densest Mediterranean water generated by  
17 extreme cooling during wintertime hurricane-strength winds – drives the thermohaline  
18 circulation, ventilates the deep layers, and changes the biogeochemical properties of the Adriatic  
19 Sea. However, modelling the dynamical properties of such dense water at the climate scale has  
20 been a challenge for decades due to the complex coastal geomorphology of the Adriatic basin not  
21 properly reproduced by existing climate models. To overcome these deficiencies, a 31-year-long  
22 simulation (1987-2017) of the Adriatic Sea and Coast (AdriSC) kilometre-scale atmosphere-  
23 ocean model is used to analyse the main NAddW dynamical phases (i.e., generation, spreading  
24 and accumulation). The study highlights four key results. First, during winter, the NAddW  
25 densities are higher in the shallow northern Adriatic shelf than in the deeper Kvarner Bay –  
26 where 25-35% of the overall NAddW are found to be generated – due to a median bottom  
27 temperature difference of 2°C between the two generation sites. Second, the NAddW mass  
28 transported across most of the Adriatic peaks between February and May, except along the  
29 western side of the Otranto Strait. Third, for the accumulation sites, the bottom layer of the  
30 Kvarner Bay is found to be renewed annually while the renewal occurs every 1–3 years in the  
31 Jabuka Pit and every 5–10 years in the deep Southern Adriatic Pit. Fourth, the NAddW  
32 cascading and accumulation is more pronounced during basin-wide high-salinity conditions  
33 driven by circulation changes in the northern Ionian Sea.

**34 Plain Language Summary**

35 The densest water in the Mediterranean Sea known as the North Adriatic Dense Water (NAddW)  
36 forms during severe winter wind events in the northern Adriatic. This phenomenon which brings  
37 oxygen-rich waters to the sea bottom, plays a vital role in sustaining life in the Adriatic Sea.  
38 However, due to the complex geography of the Adriatic, accurate representation of NAddW is  
39 very challenging and requires fine-resolution atmosphere-ocean models such as the Adriatic Sea  
40 and Coast (AdriSC) model. Here, the AdriSC historical simulation is used to study NAddW  
41 generation, spreading and accumulation. The findings reveal that about a third of NAddW is  
42 produced in the Kvarner Bay which is a deeper and warmer than the Northern Adriatic shelf.  
43 Further, it is found that NAddW spreads over most of the Adriatic between February and May  
44 bringing dense waters to the bottom of the accumulation sites, which are renewed annually in the  
45 northern Adriatic, up to every 3 years in the middle Adriatic pit, and up to every decade in the  
46 Southern Adriatic Pit. Lastly, the study highlights that NAddW spreading and accumulation are  
47 significantly enhanced during periods of higher salinity across the Adriatic, a phenomenon  
48 driven by water exchanges with the Ionian Sea.

## 49 1 Introduction

50 The Adriatic Sea is a semi-enclosed basin located in the northernmost part of the central  
51 Mediterranean Sea (Fig. 1). Its diverse and complex geomorphological characteristics (i.e.  
52 orography, bathymetry and coastline) influence a wide variety of atmospheric and oceanic  
53 processes ranging from long-term dynamics on larger spatial scales (e.g. thermohaline  
54 circulation) to short-term phenomena on smaller spatial scales (e.g. extreme wind events, dense  
55 water generation, river plume dynamics). One of the main processes driving the Adriatic  
56 thermohaline circulation is the formation of North Adriatic Dense Water (NAddW; Zore-  
57 Armanda, 1963) that occurs, in winter, over the northern Adriatic shelf and the Kvarner Bay  
58 during extreme bora events – i.e., downslope winds strongly influenced by the complex north-  
59 eastern Adriatic coastal orography and associated with hurricane-strength gusts up to  $50 \text{ m s}^{-1}$   
60 (Belušić and Klaić, 2004). In the last 40 years, the Adriatic dense water dynamics has mostly  
61 been derived from observations (Artegiani and Salusti, 1987; Gačić et al., 2002; Vilibić and  
62 Mihanović, 2013; Querin et al., 2016; Foglini et al., 2016; Paladini de Mendoza et al., 2022) and  
63 has been summarized in the review study of Vilibić et al. (2023) as follows. First, the NAddW  
64 formation is known to be preconditioned by three main factors: the bora-induced surface heat  
65 losses, the northern Adriatic river fresh water influxes, and the advection of more saline water  
66 masses from the Ionian Sea. Second, the generated dense water is known to spread towards the  
67 Strait of Otranto along the western Adriatic coast at the sea bottom beneath the Po River plume  
68 and the Western Adriatic Current. Then, along this path, dense water is known to be partly  
69 collected within the ~280-m-deep Jabuka Pit and cascading, mostly through the Bari Canyon,  
70 into the ~1230-m-deep Southern Adriatic Pit (SAP). Finally, jointly with the Adriatic Deep  
71 Water (AddW) generated in the SAP through open ocean convection, the remaining part of the  
72 NAddW leaves the Adriatic basin through the Strait of Otranto towards the northern Ionian Sea.  
73 Additionally, both NAddW and AddW have been documented to strongly influence the  
74 Adriatic–Ionian thermohaline circulation and regime changes as well as the biogeochemistry of  
75 the Adriatic Sea (Boldrin et al., 2009; Bensi et al., 2013; Gačić et al., 2010; Batistić et al., 2014;  
76 Jasprica et al., 2022).

77 In terms of numerical modelling, till recently, three different types of approaches have  
78 been used to study the Adriatic dense water dynamics. First, short-term simulations (up to 1-2  
79 weeks) have been performed with fine-resolution ocean models using different types of  
80 atmospheric forcing (e.g., Dorman et al., 2007; Ličer et al., 2016). Then, longer simulations (up  
81 to 8 years) were implemented with the aim to investigate the interannual variability of the  
82 Adriatic dense waters (e.g., Mantziafou and Lascaratos, 2008; Oddo and Guarnieri, 2011;  
83 Mihanović et al., 2018). Compared to the short-term simulations, they used either much coarser  
84 (horizontal and vertical) resolutions in the ocean and/or much coarser atmospheric forcing such  
85 as the ERA40 or ERA5 reanalyses from the European Centre for Middle-range Weather Forecast  
86 (ECMWF). Some of these simulations also imposed an inappropriate freshwater climatology in  
87 the northern Adriatic basin. Finally, the multi-decadal NAddW dynamics has also been  
88 investigated with the Mediterranean Coordinated Regional Downscaling Experiment Regional  
89 Climate Models (Med-CORDEX RCMs; Ruti et al., 2016) for the 1980–2012 period (Dunić et  
90 al., 2019). However, due to their insufficient horizontal resolution in both the ocean (order of 10  
91 km) and the atmosphere (order of 25 to 50 km), these RCMs were not capable of properly  
92 reproducing dense water formation in the northern Adriatic shelf which resulted in a noticeable  
93 ocean temperature overestimation within the NAddW accumulations sites (Jabuka Pit and SAP).

94 The kilometre-scale atmosphere-ocean Adriatic Sea and Coast (AdriSC) climate model  
95 has thus been recently implemented by Denamiel et al. (2019) with the aim to provide a better  
96 representation of the Adriatic dynamics and quantify the impacts of climate change. First, the  
97 added value of the kilometre-scale approach has been tested with short-term simulations  
98 demonstrating that the AdriSC climate model was better suited to represent the complex Adriatic  
99 atmosphere-ocean dynamics during extreme events than coarser models (Denamiel et al., 2020a,  
100 b, 2021a). Then, two 31-year-long simulations were performed with the AdriSC climate model:  
101 one during the historical period (1987-2017) and one during the future period (2070-2100) for a  
102 Representative Concentration Pathways (RCP) 8.5 scenario. Finally, the historical AdriSC  
103 simulation was successfully evaluated against in situ and remote-sensing products in both  
104 atmosphere (Denamiel et al., 2021b) and ocean (Pranić et al., 2021). Compared to the state-of-  
105 the-art Mediterranean and Adriatic models, the AdriSC climate model was demonstrated to not  
106 only reduce atmosphere-ocean biases but also to better reproduce the Adriatic Sea dynamics,  
107 including the quasi-decadal salinity and current oscillations (Denamiel et al., 2022) driven by the  
108 Adriatic-Ionian Bimodal Oscillating System (BiOS; Gačić et al., 2010; Civitarese et al., 2023),  
109 the NAddW dynamics in 2015 (Pranić et al., 2023) and the 31-year atmosphere-ocean trends and  
110 variability (Tojčić et al., 2023).

111 Following the studies demonstrating the skills of the AdriSC climate model, the aim of  
112 this research is to investigate, for the first time, the multi-decadal Adriatic dense water dynamics  
113 during the 1987-2017 period, based on climatological analyses of the AdriSC dense water results  
114 at 1-km horizontal resolution. The article is structured as follows. The AdriSC model and the  
115 methods used for the climatology analyses are described in Section 2 while the results for the  
116 generation, spreading and accumulation of the dense waters are presented in Section 3. The main  
117 findings of the study are further discussed in Section 4.

## 118 **2 Model and Methods**

### 119 **2.1 Adriatic Sea and Coast (AdriSC) model**

120 The kilometre-scale atmosphere-ocean Adriatic Sea and Coast (AdriSC; Denamiel et al.,  
121 2019) climate model is based on the Coupled Ocean–Atmosphere–Wave–Sediment Transport  
122 (COAWST) modelling system (Warner et al., 2010). It consists of the Weather Research and  
123 Forecasting (WRF; Skamarock et al., 2005) atmospheric model used with two nested grids at 15  
124 and 3 km of horizontal resolution, respectively, one-way coupled with the Regional Ocean  
125 Modelling System (ROMS; Shchepetkin and McWilliams, 2009) ocean model, also used with  
126 two nested grids at 3 km and 1 km resolution, respectively. Both models use terrain following  
127 coordinates in the vertical with 58 levels refined near the land in WRF (Laprise, 1992) and 35  
128 levels refined near the surface and bottom of the ocean in ROMS. More detailed descriptions of  
129 the AdriSC model, as well as the evaluation of the AdriSC climate simulation against  
130 observations, can be found in Denamiel et al. (2019, 2021b) and Pranić et al. (2021).

131 Importantly for the Adriatic dense water dynamics, Denamiel et al. (2022) demonstrated  
132 that the AdriSC salinity and ocean current speed signals can be explained (except in the deepest  
133 part of the SAP) by the BiOS-driven Adriatic phases – up to 61% and 9% (respectively) in the  
134 intermediate layer and up to 37% and 31% (respectively) at the bottom. These phases  
135 approximately present a 2-year lag compared to the BiOS signal in the Ionian Sea and are  
136 anticyclonic for the 1990–1999 and 2007–2011 periods and cyclonic for the 1987-1989, 2000–

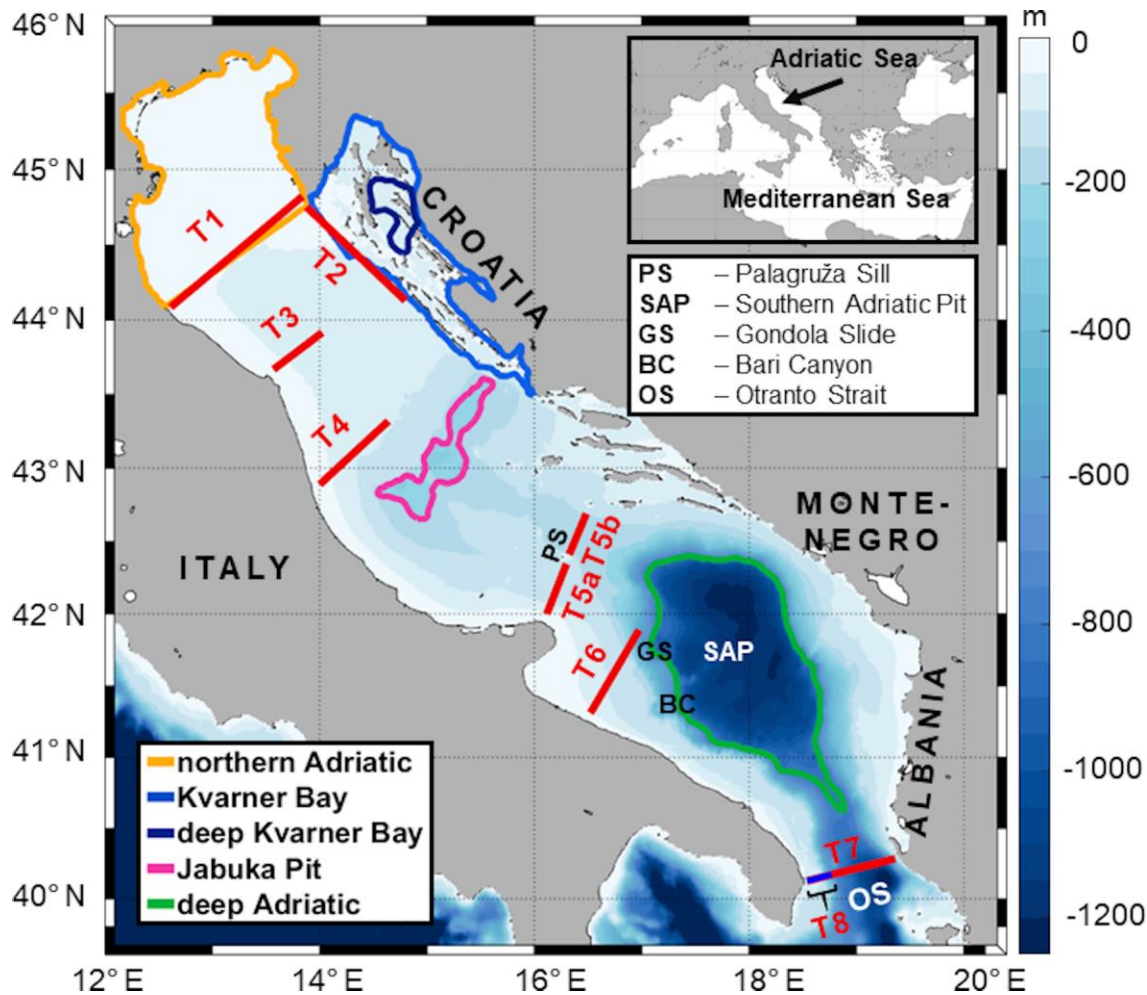
137 2006 and 2012–2017 periods. Denamiel et al. (2022) also pointed out that, due to the influence  
138 of extraordinary Eastern Mediterranean Transient (EMT; Roether et al., 2007) conditions in the  
139 1990s, the strongest anticyclonic BiOS-driven phase in the AdriSC model occurred during the  
140 1990-1999 period. Further, Tojčić et al. (2023) analysed the AdriSC atmosphere-ocean trends  
141 and variability for the 1987-2017 period and found positive salinity trends over the entire  
142 Adriatic Sea – particularly strong in the intermediate layer over the Jabuka Pit and at the bottom  
143 of the dense water generation sites – associated with a shallowing of the advection of the saline  
144 Levantine Intermediate Water inflow into the Adriatic, a decrease of the AdDW outflow, and a  
145 shrinking plus weakening of the Southern Adriatic Gyre at the centre of the SAP.

146 In this study, the daily bottom potential density anomalies (PDAs) are calculated with the  
147 daily bottom temperature and salinity extracted from the 1-km ocean results of the 31-year  
148 AdriSC historical simulation (1987-2017), and the function available within the NCAR  
149 Command Language (NCL) library (Levitus et al., 1994a, 1994b; Dukowicz, 2000;  
150 <https://www.ncl.ucar.edu/>). Further, throughout the analyses, dense water is considered, in the  
151 Adriatic Sea, for PDAs equal to or larger than  $29.2 \text{ kg m}^{-3}$  based on previous NAddW research  
152 (e.g., Mantziafou and Lascaratos, 2008; Janeković et al., 2014; Vilibić et al., 2018).

## 153 2.2. Climatological analysis

154 The climatological analyses are performed for the three main dynamical phases of the  
155 dense water dynamics: generation, spreading and accumulation. The analyses of the dense water  
156 generation are carried out for the two generation sites – northern Adriatic (NA) and Kvarner Bay  
157 (KB; Fig. 1). The results are presented in the form of daily time series of subdomain averaged  
158 bottom PDA, temperature and salinity for the whole time period of the simulation. The  
159 maximum bottom PDAs are calculated for each point of the subdomains in January, February  
160 and March (JFM). Also, the day of the year (DOY) in which the maximum PDA value occurred  
161 is considered. The results are presented as: 1) probability density functions (PDFs) derived with  
162 a kernel-smoothing method for the maximum bottom PDAs as well as bottom temperature and  
163 salinity during the DOYs of maximum PDAs, and 2) box plots of yearly maximum PDA and  
164 associated DOY, as well as bottom temperature and salinity during these DOYs (in Supplemental  
165 Material). A kernel-smoothing method (Bowman and Azzalini, 1997) is used to calculate the  
166 probability density estimate based on a normal kernel function and is evaluated for 100 equally  
167 spaced points.

168 Concerning the spreading phase, the analyses are performed for nine transects (T1, T2,  
169 T3, T4, T5a, T5b, T6, T7, T8) which are defined along the known dense water pathways. The  
170 outward dense water flow rates are calculated only for the bottom layer and are obtained by  
171 multiplying the bottom velocities normal to the transect by the bottom PDAs along each transect.  
172 The results are shown as monthly time series of cumulative dense water mass transported  
173 outward through the transects – i.e., monthly sum of the outward dense water flow rates. The  
174 obtained quantity is defined as positive in the northwest direction for all transects except T2, for  
175 which it is positive in the northeast direction. Additionally, the climatology of the monthly  
176 bottom dense water mass transported outward is also presented as bar plots for all transects.



177  
 178 **Figure 1.** Bathymetry of the AdriSC 1-km model domain with indicated geographical terms, as  
 179 well as the subdomains and transects (red lines) used to study the Adriatic dense water multi-  
 180 decadal dynamical properties during the 1987-2017 period.

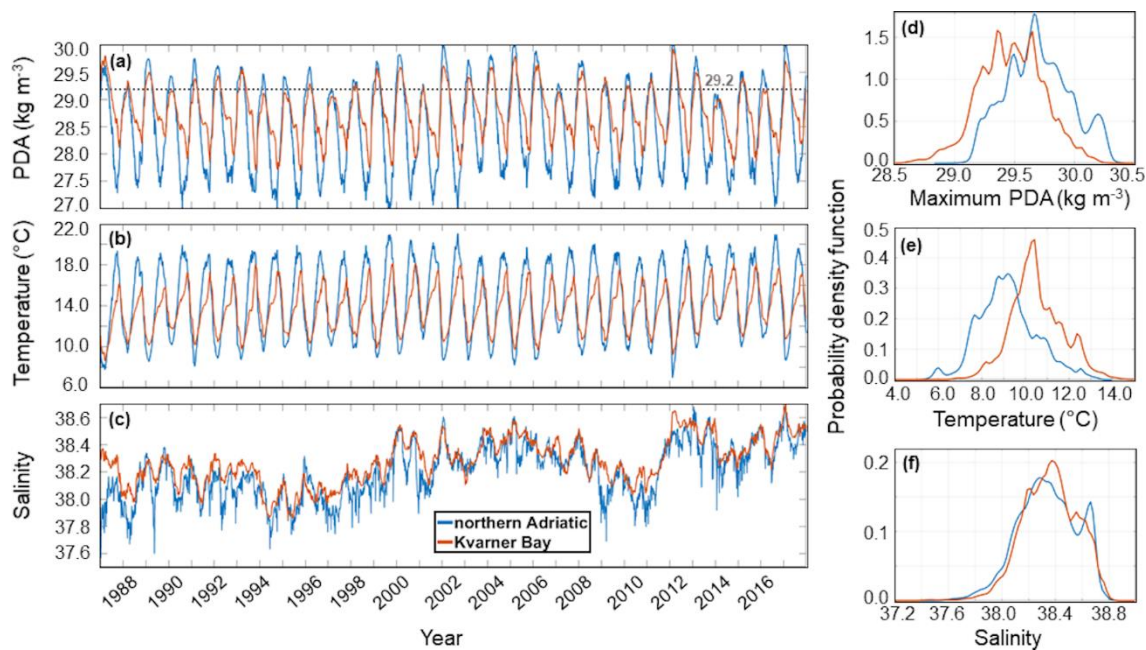
181 To quantify the dense water accumulation for the whole simulation period, several  
 182 analyses were conducted for three accumulation sites (subdomains) – deep Kvarner Bay (DKB)  
 183 with depths above 80 m, Jabuka Pit (JP) with depths above 200 m and deep Adriatic (DA) with  
 184 depths above 1000 m encompassing the SAP (Fig. 1). The JP and the SAP are well-known and  
 185 well-researched dense water accumulation sites (e.g., Zore-Armanda, 1963; Querin et al., 2016),  
 186 while dense waters generated in the Kvarner Bay are gravitationally attracted in DKB which is  
 187 much deeper than the adjacent open northern Adriatic shelf. Firstly, an mp4 animation of the  
 188 spatial daily results of the bottom PDA over the Adriatic Sea and the time series of subdomain-  
 189 averaged bottom PDAs (Movie S1) as well as the time series of subdomain-averaged bottom  
 190 temperature and salinity are analysed. Then, the maximum bottom PDA and associated DOY as  
 191 well as the bottom temperature and salinity during these DOYs (in Supplemental Material) are  
 192 presented as box plots. Lastly, the monthly-averaged bottom PDAs as well as bottom  
 193 temperature and salinity (in Supplemental Material) are presented as box plots (without outliers).

### 194 3 Results

195

## 3.1 Dense water generation

196 The process of dense water generation is investigated first by analysing the daily time  
 197 series of averaged bottom PDA, temperature and salinity for the NA and KB subdomains (Fig.  
 198 2). The seasonal variability of all three variables in NA is larger compared to KB. In particular,  
 199 bottom PDAs in NA vary between 27.0 and 30.0  $\text{kg m}^{-3}$ , while in KB they range from 27.7 to  
 200 29.9  $\text{kg m}^{-3}$  (Fig. 2a). Also, PDA maximums are often smaller in KB than in NA (by 0.1–0.4  $\text{kg m}^{-3}$ ).  
 201  $\text{m}^{-3}$ ). The time series of PDA in NA reveals a sharp increase during winter reaching a peak in  
 202 February, followed by a sharp decrease until the end of summer when the PDA minimums are  
 203 produced. In KB, a smaller secondary peak in PDA is present during summer, associated with  
 204 dense water accumulation in the deepest KB sections. In autumn, the larger PDA simulated in  
 205 KB compared to NA indicates delayed mixing of the entire water column due to the greater  
 206 depths within KB. Dense waters with PDA equal to or larger than 29.2  $\text{kg m}^{-3}$  are generated  
 207 throughout most of the years, except for 2014 in NA and 1990, 1994–1997, 2007 and 2014 in  
 208 KB. The years with the strongest dense water generation (indicated by a PDA maximum larger  
 209 than 29.5  $\text{kg m}^{-3}$ ) are 1989, 1991, 1999, 2000, 2002–2006, 2008, 2012, 2013 and 2017 in NA,  
 210 and 1987, 1989, 1993, 1999, 2000, 2002, 2004–2006, 2008, 2012, 2013 and 2017 in KB.



211

212 **Figure 2.** Daily time series of bottom (a) PDA, (b) temperature and (c) salinity for the northern  
 213 Adriatic and Kvarner Bay subdomains during the 1987–2017 period. Probability density  
 214 functions of (d) maximum bottom PDA, as well as bottom (e) temperature and (f) salinity for the  
 215 DOY with maximum PDA in the northern Adriatic and Kvarner Bay subdomains during the JFM  
 216 seasons of the 1987–2017 period.

217 Bottom temperature varies between 6.5 and 21.0  $^{\circ}\text{C}$  in NA and between 8.0 and 17.0  $^{\circ}\text{C}$   
 218 in KB (Fig. 2b). Temperature peaks are mostly reached in late autumn in KB, while in NA they  
 219 occur in summer, reacting faster to changes in surface heat flux due to its shallower depth. The  
 220 lowest temperatures were produced during the extreme winter of 2012 in both subdomains.  
 221 Bottom salinity values are overall larger in KB than in NA (Fig. 2c). In the 1987–1999 period,

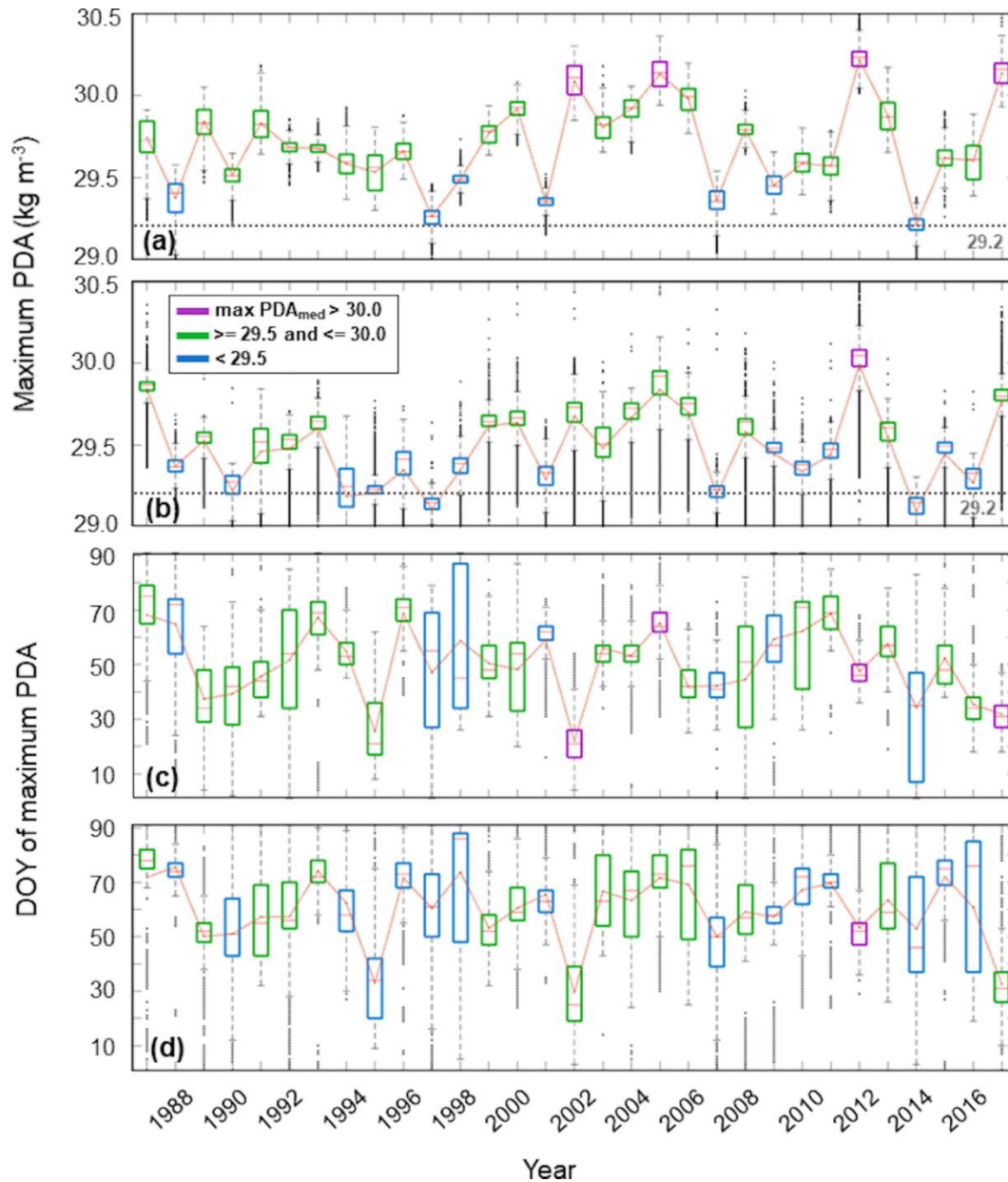
222 salinity varies between 37.6 and 38.4 in NA and between 38.0 and 38.4 in KB. Larger salinities  
223 are simulated in the 2000–2008 period in both subdomains, followed by a decrease until 2011.  
224 Then, a steep increase occurred leading to large salinities in the 2012–2013 period. Notably, in  
225 2012, salinity in KB reached a peak larger than in NA (by more than 0.1), while the temperature  
226 was higher by approximately 2.5 °C. Consequently, very close extreme values of PDA were  
227 simulated in the two generations sites. Similarly, in 1987, substantially larger salinity in KB  
228 resulted in larger PDAs compared to NA. However, even though 1987 has been documented to  
229 have strong dense water formation events (Vilibić and Orlić, 2001), these AdriSC results should  
230 be considered with caution due to possible influence of the initial conditions imposed only 2  
231 months before January 1987 during the short spin-up period. Further, a slight salinity decrease  
232 occurred after 2013 in both subdomains, followed by an average increase and peaking at 38.7 in  
233 2017. Finally, for both generation sites, positive trends (Tojčić et al., 2023) and influence of the  
234 quasi-decadal BiOS-driven phases (Denamiel et al., 2022) are noticeable in the AdriSC bottom  
235 salinity time series.

236 In order to examine the differences in the behaviour of thermohaline parameters between  
237 the two generation sites, the PDFs of maximum bottom PDA, as well as bottom temperature and  
238 salinity for the DOY with maximum PDA during the winter (JFM) seasons of the 1987–2017  
239 period, are also presented in Fig. 2. Maximum PDAs are generally larger in NA where the  
240 highest probabilities are obtained for the PDAs around 29.7 kg m<sup>-3</sup>, while in KB the most  
241 probable PDAs range between 29.3 and 29.6 kg m<sup>-3</sup> (Fig. 2d). Temperatures are generally higher  
242 in KB, with the highest probabilities for values around 10–11 °C, whereas in NA, around 9 °C  
243 (Fig. 2e). Conversely, the salinity PDFs are very similar in both subdomains, with salinities  
244 mostly distributed between 37.8 and 38.8 (Fig. 2f). Slightly higher probabilities are found for  
245 salinities around 38.4 in KB and below 38.3 in NA. Hence, dense water generated in NA is  
246 denser compared to KB mainly due to its lower temperatures, while the salinity difference  
247 between the two formation sites remains small. It should be noticed that despite the maximum  
248 heat losses occurring over KB during the dense water generation (e.g., Dorman et al., 2007;  
249 Janeković et al., 2014; Denamiel et al., 2021a), the lowest bottom temperatures are found in NA  
250 which is 3 times shallower than the deepest part of the KB.

251 The annual climatology of maximum bottom PDA and associated DOY of maximum  
252 PDA during the JFM season between 1987 and 2017 is presented in the form of box plots for  
253 both subdomains (Fig. 3 and 4). In NA, the years with the smallest maximum PDAs (median of  
254 maximum PDAs < 29.5 kg m<sup>-3</sup>) and therefore the weakest dense water generation are: 1988,  
255 1997, 1998, 2001, 2007, 2009 and 2014 (Fig. 3a). The years with the strongest dense water  
256 generation (median of maximum PDAs > 30.0 kg m<sup>-3</sup>) are: 2002, 2005, 2012 and 2017. The  
257 remaining majority of the years belongs to the moderate category with maximum PDAs between  
258 29.5 and 30.0 kg m<sup>-3</sup>. In KB, distributions of maximum PDAs are generally smaller than those  
259 in NA (Fig. 3b). Median maximum PDAs larger than 30.0 kg m<sup>-3</sup> are produced only in  
260 February–March 2012, which is confirmed by sparse observations in that area indicating a  
261 maximum PDA of around 30.0 kg m<sup>-3</sup> (Mihanović et al., 2013; Raicich et al., 2013). In one half  
262 of the remaining years, PDAs range between 29.5 and 30.0 kg m<sup>-3</sup>, while in the other half, they  
263 are smaller than 29.5 kg m<sup>-3</sup>.

264 The median of the DOY of maximum PDA in NA varies between 25 and 70, revealing  
265 the interannual differences in the timing of the dense water generation. For example, in 2002, the

266 major dense water generation event occurred in January without further increases in PDA  
 267 afterward. Conversely, in 2011, the highest PDA is produced in March, indicating substantial  
 268 late-winter cooling. Further, some years have a wide range in the distributions of the DOY of the  
 269 maximum PDA, suggesting the occurrence of either several presumably weak dense water events  
 270 in different parts of NA or a slow transport of dense water in the bottom layers of the northern  
 271 Adriatic shelf (Vilibić et al., 2008). The box plots of the DOY in KB are similar to those for NA  
 272 but with a slight prevalence of the later part of the JFM period. Also, years with wider range in  
 273 distributions of the DOY are present in KB which indicates the existence of several cooling  
 274 events.



275

276 **Figure 3.** Box plots of maximum bottom PDA and DOY of maximum PDA for the (a, c)  
 277 northern Adriatic (NA) and (b, d) Kvarner Bay (KB) subdomains in the 1987–2017 period. The

278 red line inside each box plot denotes the median of the distribution. The orange dotted line  
279 connects the mean values of the distributions.

### 280 3.2. Dense water spreading

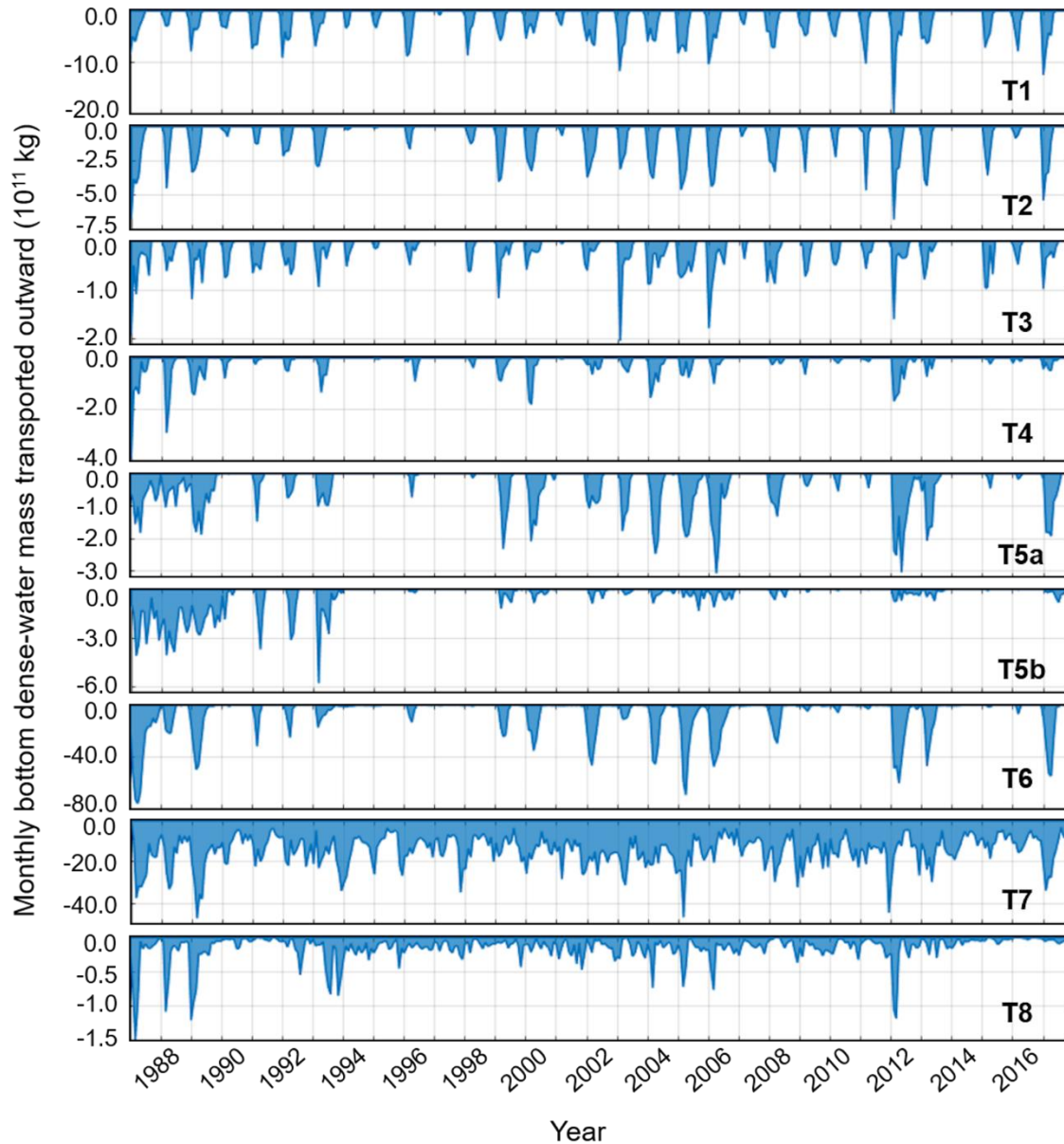
281 The spreading of dense water is analysed along different transects across the Adriatic Sea  
282 (Fig. 1). First, the time series of monthly bottom dense water mass transported outward through  
283 the nine transects are presented in Fig. 4. At T1, located on the southern edge of the northern  
284 Adriatic, indicating the dense water outflow solely from the northern Adriatic, the transported  
285 dense water mass mostly varies around  $-10.0 \cdot 10^{11}$  kg, slightly surpassing this value in 2003 and  
286 2017. The largest mass of dense water is transported through T1 in February 2012, sharply  
287 peaking at  $-20.0 \cdot 10^{11}$  kg. The amounts of transported dense water mass through T2, marking the  
288 boundary between the open sea and the northern half of the Kvarner Bay and indicating dense  
289 water mass outflow from the Kvarner Bay only, mostly vary around  $-5.0 \cdot 10^{11}$  kg and  
290 exceptionally to  $-6.8 \cdot 10^{11}$  kg in February 2012. A comparison between T2 and T1 bottom dense  
291 water mass outflow, suggests that the outflow from the Kvarner Bay is 2–3 times lower than the  
292 outflow from the northern Adriatic, attributing 25–35% of the total generated dense waters to the  
293 Kvarner Bay. This estimate is smaller than the previously quantified contribution of the Kvarner  
294 Bay to the total dense water formation during winter 2012 found to be around 40% by Janeković  
295 et al. (2014). This might be linked to differences in methodology (mass vs. volume transports)  
296 but also to the fact that 2012 was an exceptional year for dense water generation with a very dry  
297 preconditioning resulting in higher than usual salinities and, hence, PDAs in the coastal Kvarner  
298 Bay (Mihanović et al., 2013).

299 Further southeast, at T3 in the middle Adriatic, the bottom dense water mass varies  
300 around  $-1.0 \cdot 10^{11}$  kg, while larger values around  $-2.0 \cdot 10^{11}$  kg are obtained in 2003, 2006 and  
301 2012. The decrease possibly reflects enhanced mixing between dense waters and ambient waters  
302 known to occur in this region (Vilibić and Mihanović, 2013) and strongly modify the dense  
303 water outflow. The T4 transect, located north of the Jabuka Pit in the middle Adriatic, shows  
304 mostly smaller amounts of transported dense water mass except in 1988, 2000 and 2012 (near -  
305  $2.0 \cdot 10^{11}$  kg or larger).

306 Significant differences are evident between the two transects, T5a and T5b, located in the  
307 Palagruža Sill and divided by the island of Palagruža. Until the mid-1990s, the monthly  
308 transported dense water mass is much larger at T5b (reaching  $-6.0 \cdot 10^{11}$  kg) than at T5a (reaching  
309  $-2.0 \cdot 10^{11}$  kg), after which there is a period of reduced dense water transport until 1999. From  
310 2000 to 2017, a reversal occurs with the transported dense water mass being larger at T5a  
311 (reaching  $-3.0 \cdot 10^{11}$  kg) compared to T5b ( $> -1.0 \cdot 10^{11}$  kg). This may indicate a major change in  
312 dense water dynamics over the northern Adriatic shelf – e.g., due to circulation changes or  
313 differences between dense water and the ambient water densities and potential shallowing of the  
314 dense water outflow – as the dense water arriving through T5b cascades initially to the Jabuka  
315 Pit before being transported along the deepest sections of the Palagruža Sill (Vilibić et al., 2004).  
316 In contrast, dense waters arriving through T5a are directly coming from the northern Adriatic  
317 shelf, detouring the Jabuka Pit along the western shelf.

318 At T6, in the northwestern part of the southern Adriatic, very large amounts of dense  
319 water mass are transported in specific years (1989, 2000, 2002–2006, 2008, 2012, 2013 and

320 2017), with the largest mass transported in April 2005 reaching  $-70.0 \cdot 10^{11}$  kg. This time series  
 321 resembles the one at T5a, indicating that most of the dense waters are transported downslope  
 322 along the western sections of the SAP towards its deeper layers (e.g., Gondola Slide, Bari  
 323 Canyon, Foglini et al., 2016; Langone et al., 2016).



324

325 **Figure 4.** Time series of monthly bottom dense water mass transported outward at transects: T1,  
 326 T2, T3, T4, T5a, T5b, T6, T7 and T8 for the 1987–2017 period.

327 For transects T1-T6, the AdriSC bottom dense water mass outflows present strong quasi-  
 328 decadal variations which, as demonstrated in Denamiel et al. (2022), are linked to both the EMT  
 329 substantially lowering the Adriatic salinities in the 1990s, and the BiOS-driven phases

330 influencing bottom salinity and ocean current speed variations across the Adriatic basin (e.g.,  
331 larger dense water mass outflow during the 2000–2006 strong cyclonic BiOS-driven phase).

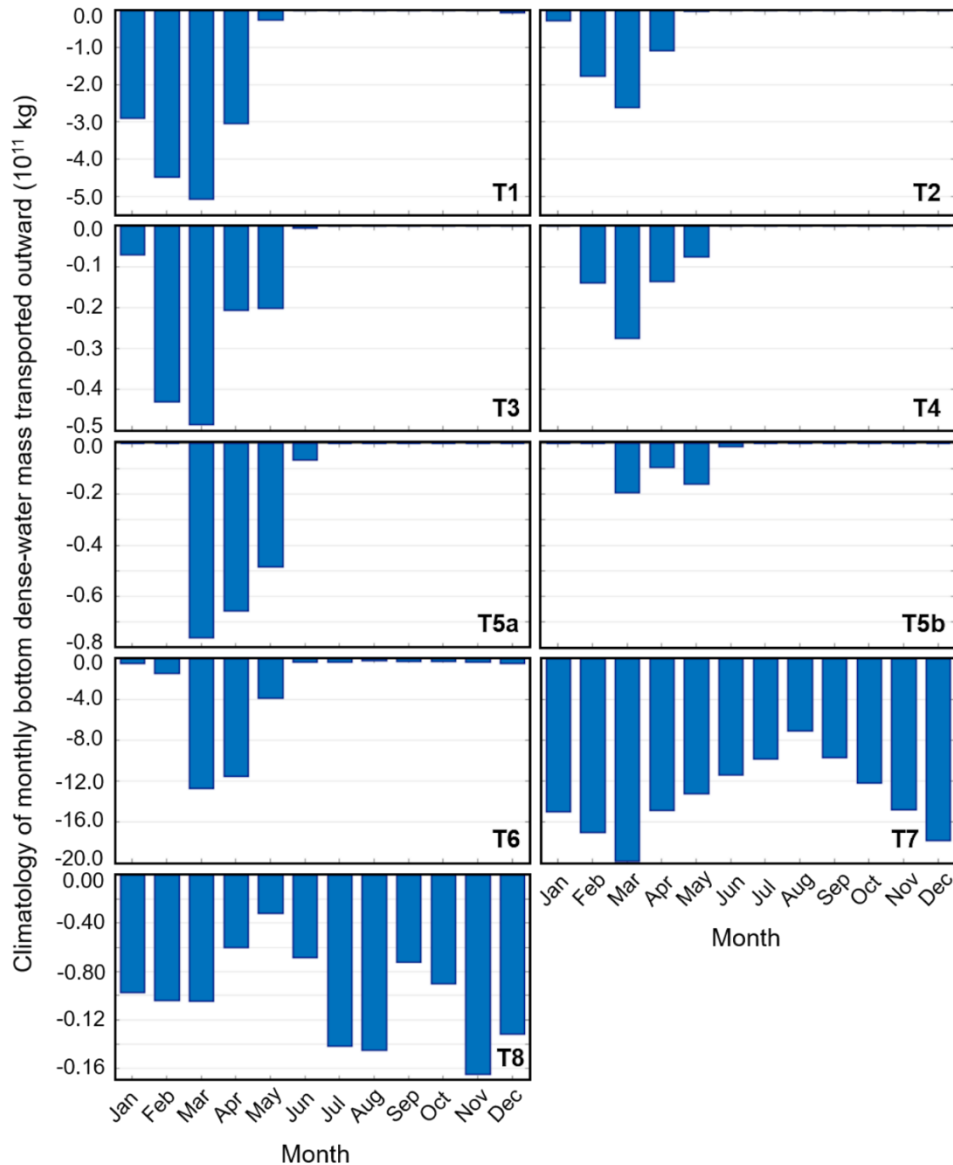
332 The remaining transects, T7 and T8, are located in the Strait of Otranto, where T7 is a  
333 full-length transect and T8 is a shorter transect covering the shelf on the western coast. The time  
334 series reveal completely different dynamics at T7 and T8 compared to the other transects: the  
335 dense water transport at T7 is predominantly driven by open-ocean convection in the SAP (e.g.,  
336 Bensi et al., 2013; Querin et al., 2013), while dense water transport at T8 is also strongly  
337 influenced by the properties of the dense water coming over the Palagruža Sill. At least around -  
338  $5.0 \cdot 10^{11}$  kg is transported each month through T7 ( $-15.0 \cdot 10^{11}$  kg on average), with a few  
339 exceptional peaks of  $-47.0 \cdot 10^{11}$  kg. At T8, the monthly bottom dense water mass is about -  
340  $0.5 \cdot 10^{11}$  kg. In some few years, such as 2012, the values reach  $-1.0 \cdot 10^{11}$  kg at the beginning of  
341 the year. Notably, the substantial bottom dense water mass outflow in 2012 at T6 and T7  
342 indicates massive dense water production in the northern Adriatic during the winter, being  
343 capable to sustain both the strong downslope currents along the western SAP of its denser  
344 fraction and strong bottom current along the shelf of its lighter fraction, extending up to the Strait  
345 of Otranto. Indeed, a rapid BiOS reversal has been demonstrated after massive dense water  
346 outflow in 2012 (Gačić et al., 2014). The same refers to 1987, which is also recognized as a year  
347 when massive dense water production was observed (Vilibić and Orlić, 2001). However, in  
348 certain years (1992–1993) the dense water outflow at T8 occurs in summer or autumn, indicating  
349 that some other mechanism than bottom density current is responsible for transport of these  
350 waters.

351 The monthly climatology of the bottom dense water mass transported outward at the nine  
352 transects is examined for the 1987–2017 period (Fig. 5). At T1, the largest amounts of dense  
353 water mass are transported from January to April and range from  $-2.9 \cdot 10^{11}$  kg (January) to -  
354  $5.1 \cdot 10^{11}$  kg (March). Similar distribution is obtained at T2 but with smaller values ranging from -  
355  $1.8 \cdot 10^{11}$  to  $-2.6 \cdot 10^{11}$  kg. At T3, the transported dense water mass is the largest from February to  
356 May, ranging from  $-0.2 \cdot 10^{11}$  kg to almost  $-0.5 \cdot 10^{11}$  kg, while T4 shows smaller amounts,  
357 reaching almost  $-0.3 \cdot 10^{11}$  kg.

358 At T5a, the largest values are obtained in March (approximately  $-0.8 \cdot 10^{11}$  kg) and they  
359 further decrease until June. The neighbouring transect T5b, shows its largest transported dense  
360 water mass in March and May (down to  $-0.2 \cdot 10^{11}$  kg), generally having smaller values than T5a.  
361 This double maximum may be related to direct outflow over the deepest parts of the Palagruža  
362 Sill occurring simultaneously in March, with the outflow along southern sections of the sill  
363 (T5a), and a delayed outflow of dense water originating either from old waters residing in the  
364 Jabuka Pit or from a spillover of new dense water that first cascade into the pit and then overflow  
365 the deepest parts of the Palagruža Sill (May).

366 Further southeast, at T6, the distribution peaks in March and April, reaching around  $-12.0$   
367  $\cdot 10^{11}$  kg, while in May, it reaches  $-4.0 \cdot 10^{11}$  kg, resembling the seasonality reproduced at T5a.  
368 Indeed, a delay between bottom dense water mass outflow at T1 and other transects reveals the  
369 average time needed for the dense water to travel until it cascades into the SAP. On average, it  
370 rapidly reaches the northwestern perimeter of the Jabuka Pit in less than a month, but the Jabuka  
371 Pit serves as an obstacle and collector of the densest water, after which the dense water requires  
372 an additional month to be transported downslope to the deep SAP (if having sufficiently high

373 PDA). These modelling results agree with times derived from *in situ* observations (Vilibić and  
 374 Orlić, 2001).



375

376 **Figure 5.** Climatological monthly bottom dense-water mass transported outward at transects: T1,  
 377 T2, T3, T4, T5a, T5b, T6, T7 and T8 for the 1987–2017 period.

378 At T7, the transported dense water mass remains large throughout the year, increasing  
 379 from January to March, when it reaches  $-20.0 \cdot 10^{11}$  kg, and then decreasing slowly until August  
 380 down to  $-8.2 \cdot 10^{11}$  kg, after which it increases to  $-17.8 \cdot 10^{11}$  kg in December. These two maxima  
 381 may resemble the outflow of dense water after its generation (the March maximum), while the  
 382 December maximum could result from enhanced circulation and exchange of water masses in the  
 383 Strait of Otranto, known to occur in late autumn/early winter (e.g., Mihanović et al., 2021).  
 384 Undoubtedly, the general circulation and water mass exchange between the SAP and the  
 385 northern Ionian Sea is a driver of the dense water outflow throughout the year, considering the

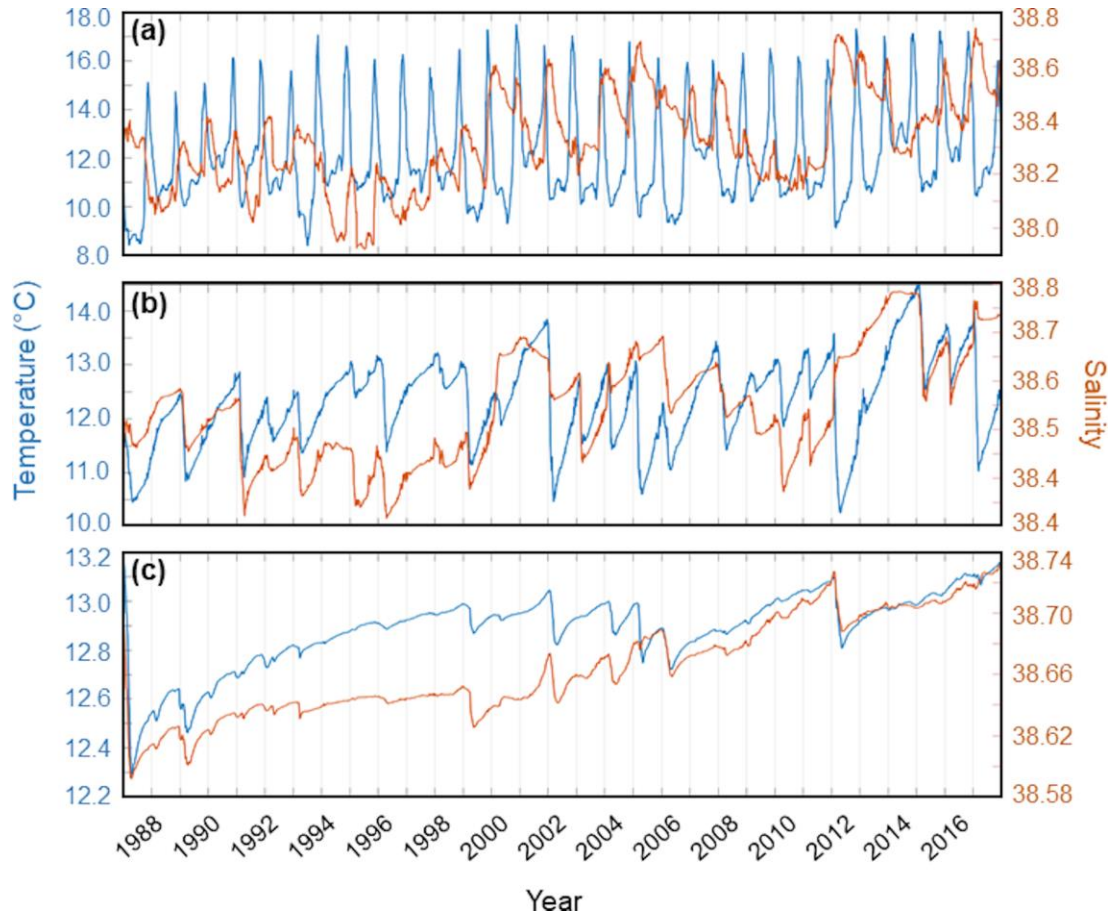
386 average capacity of the SAP to accumulate dense water is about two years (Vilibić and Orlić,  
387 2002). Finally, at T8, the bottom dense water mass outflow values remain around  $-0.10 \cdot 10^{11}$  kg  
388 from January to March, decreasing until May. Larger values are obtained in July and August,  
389 reaching down to  $-0.14 \cdot 10^{11}$  kg, while the largest transported dense water mass is produced in  
390 November ( $-0.16 \cdot 10^{11}$  kg) and December ( $-0.13 \cdot 10^{11}$  kg).

### 391 3.3. Accumulation sites

392 The accumulation of dense water during the 1987-2017 period is first investigated by  
393 analysing, in the DKB, JB and DA subdomains, both the animation (Movie S1) of daily time  
394 series of bottom PDA and the time series of bottom temperature and salinity (Fig. 6). The general  
395 pattern in DKB involves a sharp increase in PDA at the beginning of the year when the dense  
396 water generation is occurring and temperatures can drop to  $8.5$  °C due to consistent wintertime  
397 heat losses and cooling events (e.g., Artegiani et al., 1997). It is then followed by a sharp  
398 decrease at the end of the year when vertical mixing of the whole water column is occurring in  
399 late autumn (e.g., Viličić et al., 2009) and temperatures can reach  $17.5$  °C. The years with the  
400 largest PDAs ( $> 29.6$  kg m<sup>-3</sup>) and lowest winter temperatures ( $< 10$  °C) are: 1993, 2000, 2002,  
401 2004–2006, 2012 (up to  $30.0$  kg m<sup>-3</sup>) and 2017. Two PDA peaks are frequently occurring during  
402 a year, the first in February–March when the dense water formation is occurring, and the second  
403 a few months later, during the summer months. The second maximum may resemble either the  
404 post-generation spreading of dense water inside the Kvarner Bay associated with a thermohaline  
405 circulation due to the dense water sinking from the shallow to the deepest parts of the Kvarner  
406 Bay as a slow bottom density current, or the advection of dense water from the northern Adriatic  
407 shelf. The bottom salinity variations demonstrate a completely different behaviour as they are  
408 mostly driven by the EMT and the BiOS-driven phases as demonstrated in Denamiel et al.  
409 (2022): salinities within the  $37.9$ – $38.4$  range are produced during the 1987–1999 period,  
410 followed by a period of larger salinities in the  $38.2$ – $38.7$  range from 2000–2008 and, after 2008,  
411 a short period of smaller salinities occurred from 2009–2011. In 2005, 2012 and 2017, very large  
412 salinities surpassing  $38.7$  coincided with very low temperatures (down to  $9$  °C), indicating the  
413 accumulation of extremely dense waters. Further, the sharp temperature increase in late autumn  
414 typically coincides with an increase in salinity, revealing the advection of higher salinity open  
415 Adriatic waters in autumn. Salinity is generally dropping during dense water generation,  
416 indicating that the generated and advected waters to DKB are coming from shallower regions  
417 with more pronounced cooling effects. Finally, as seen in previous studies (Janeković et al.,  
418 2014; Pranić et al., 2023), the dense waters reside within the DKB for about a year.

419 In JP, PDA time series exhibits a “saw-tooth” pattern with large changes occurring every  
420 1–3 years, previously detected in shorter ocean simulations (Mihanović et al., 2018) and  
421 observations (Artegiani et al., 2001). This pattern is mostly driven by the temperature variations.  
422 During some years (e.g., 2002, 2012), the bottom temperatures present large late-winter decrease  
423 resulting from colder dense water cascading into the pit. Conversely, in years lacking this  
424 cascading phenomenon (e.g., 2001, 2014), the temperature tends to continue rising. The bottom  
425 temperatures mostly vary between  $10.5$  and  $13.5$  °C and present the largest drops in 2002 and  
426 2012. In all years except 2012, drops in temperature are associated with drops in salinity,  
427 indicating that the dense water generated in the northern Adriatic has lower salinity than the  
428 residing waters in the Jabuka Pit. Notably, in 2012, a sharp salinity increase is associated with a  
429 sharp decrease in temperature, indicating the arrival of highly saline waters in the northern

430 Adriatic during autumn 2011, reaching dense water sites in winter 2012. As previously  
 431 demonstrated, the AdriSC bottom salinity variations within the JP mostly follow the BiOS-  
 432 driven quasi-decadal oscillations and the influence of the EMT (Denamiel et al., 2022) but also  
 433 longer positive trends (Tojčić et al., 2023).

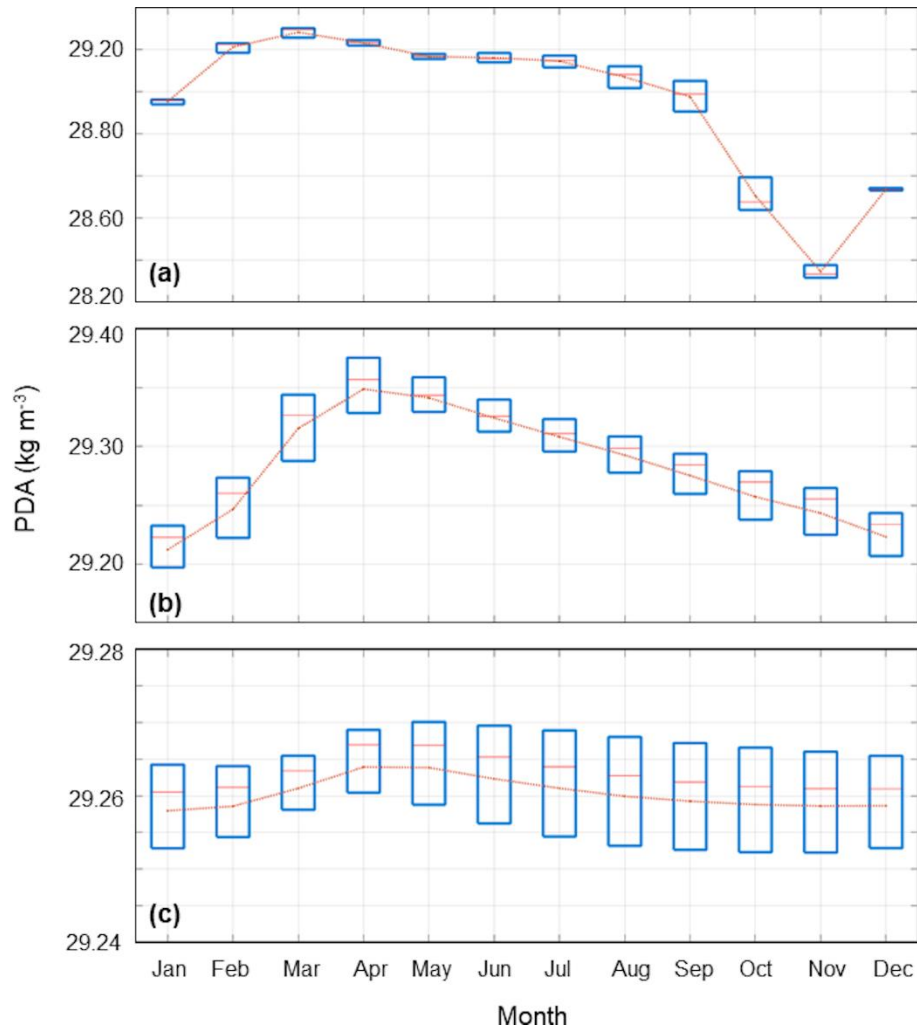


434

435 **Figure 6.** Daily time series of bottom temperature and salinity in the (a) deep Kvarner Bay  
 436 (DKB), (b) Jabuka Pit (JP) and (c) deep Adriatic (DA), during the 1987–2017 period.

437 In DA, during the 1989–2000 period PDA generally decreased to  $29.23 \text{ kg m}^{-3}$  with  
 438 smaller annual variations. After 2000, the PDA slowly increased each year until 2005, when a  
 439 very sharp rise to  $29.30 \text{ kg m}^{-3}$  occur. The next sharp increase in the DA bottom PDA values  
 440 occurred during 2012, reaching slightly less than  $29.30 \text{ kg m}^{-3}$ . Another smaller peak of bottom  
 441 PDA can be noticed in 2017, restricting the dense water cascading during this event just in the  
 442 Jabuka Pit, with much lower intensity in the Southern Adriatic Pit. Convincingly, it can be seen  
 443 that the PDA time series in DA also exhibits a “saw-tooth” pattern already measured by near-  
 444 bottom sensors at the E2-M3A buoy (Querín et al., 2016), while the AdriSC climate model  
 445 results indicate large PDA changes occurring there every 5–10 years. Interestingly, the  
 446 associated bottom temperature and salinity exhibit similar “saw-tooth” patterns. The temperature  
 447 generally ranges between 12.3 and 13.2 °C, with the largest drops occurring in 2002, 2005 and  
 448 2012 when it decreased by slightly more than 0.2 °C during winter. Salinity ranges between  
 449 38.60 and 38.73, with several larger jumps such as during 2001–2002, in 2005 and during 2011–

450 2012. In 2012, in contrast with JP, the decrease in temperature at the bottom of DA is associated  
 451 with a decrease in salinity.



452

453 **Figure 7.** Annual courses of monthly box plots of bottom PDA for the (a) deep Kvarner Bay  
 454 (DKB), (b) Jabuka Pit (JP) and (c) deep Adriatic (DA) subdomain in the 1987–2017 period. The  
 455 red line inside each box plot denotes the median of the distribution. The orange dotted line  
 456 connects the mean values of the distributions.

457 The monthly climatology of bottom PDA for the DKB, JP and DA subdomains is  
 458 presented in Figure 7, while the corresponding temperature and salinity plots may be found in  
 459 Supplemental Material (Fig. S5 and S6). In DKB, PDAs are the largest from February to May,  
 460 peaking in March at around 29.22 kg m<sup>-3</sup> (Fig. 7a). Then they decrease until May and keep  
 461 constant values for almost 3 months. This behaviour may result from either a slow dense water  
 462 spreading from the shallower parts of KB or the advection of dense water from the northern  
 463 Adriatic shelf. After September, a steep decrease in PDA occur and a minimum of around 28.24  
 464 kg m<sup>-3</sup> is reached in November when the whole water column is mixed. The temperature follows  
 465 the PDA distributions but in an inverse manner, with a minimum in March down to 10.5 °C and  
 466 a maximum in November up to 15.7 °C. Salinity shows its largest values in January and

467 February (around 38.39), after which it decreases, reaching a minimum in October of  
468 approximately 38.26, followed by a sharp increase until December and largest variability in  
469 November.

470 In JP, the smallest PDAs are produced in January around  $29.3 \text{ kg m}^{-3}$ , after which there is  
471 an increase until April, when they reach around  $29.35 \text{ kg m}^{-3}$  (Fig. 7b). Therefore, the dense  
472 water cascading into the JP lasts from February to April on average. Subsequently, from May to  
473 December, PDAs slowly decrease to around  $29.23 \text{ kg m}^{-3}$ , due to the slow mixing with the  
474 warmer and more saline intermediate waters. Temperature distributions are very similar to PDA  
475 distributions but inversed. Minimum temperatures are reached in April down to  $11.7\text{--}12.0 \text{ }^\circ\text{C}$ ,  
476 after which they increase. Salinities are larger in January and February (around  $38.56\text{--}38.57$ )  
477 followed by a sharp decrease until May down to  $38.52$ , after which they increase until December,  
478 indicating a lag of one month after the temperature changes.

479 Monthly box plots in DA reveal relatively small variations (Fig. 7c). PDAs slowly  
480 increase from February to peak around  $29.26 \text{ kg m}^{-3}$  in April and May, after which they slightly  
481 decrease until the end of the year. Indeed, these distributions indicate the possibility of dense  
482 water cascading reaching in average the bottom of the SAP between late February and May.  
483 Temperature and salinity have similar behaviour, decreasing until April and May and then slowly  
484 increasing until December. The monthly variations in median temperature and salinity are  
485 approximately  $0.5 \text{ }^\circ\text{C}$  and slightly larger than  $0.01$ , respectively.

## 486 **4 Discussion**

487 This paper, for the first time, analyses and quantifies the Adriatic multi-decadal bottom  
488 dense water dynamics coming from kilometre-scale ocean simulations. For that, the 31-year-long  
489 AdriSC atmosphere-ocean historical climate simulation (1987-2017) with horizontal resolution  
490 of  $1 \text{ km}$  has been used. Hereafter, three key results are further discussed and a basic classification  
491 of the Adriatic dense water events is proposed.

### 492 **4.1 Dense water generation in the Kvarner Bay**

493 The AdriSC model is the first model to properly simulate the multi-decadal dense water  
494 generation within the Kvarner Bay. In particular, in this study, it was found that the differences  
495 in maximum PDA during winter months between the open northern Adriatic shelf and the  
496 Kvarner Bay dense water generation sites are primarily influenced by a median difference of  $2^\circ\text{C}$   
497 in temperature while the salinity difference is neglectable. The difference in temperature between  
498 the two generation sites is explained by much larger ocean depths in the Kvarner Bay, so that the  
499 cooling rates during severe bora outbreaks – simulated to reach their maximum in the Kvarner  
500 Bay by the AdriSC model (Denamiel et al., 2020a, b, 2021a) – are found to be less important for  
501 the temperature decrease (and thus, for the PDA increase) than the volume of the ocean to be  
502 cooled. However, the fact that no major salinity difference exists between the two generation  
503 sites contrasts with previous modelling results. Indeed, the other modelling study spanning over  
504 several years – that analysed the results of a ROMS ocean model with a  $2 \text{ km}$  horizontal  
505 resolution forced by  $8 \text{ km}$  atmospheric fields extracted from the Aladin/HR hydrostatic weather  
506 prediction model – found that dense waters generated in the Kvarner Bay were less salty than the  
507 dense waters generated on the northern Adriatic shelf (Mihanović et al., 2018). The reason for

508 the difference in salinity between the two models can be attributed to the several times higher  
509 water exchanges between the Kvarner Bay and the open sea reproduced by the AdriSC model  
510 (Denamiel et al., 2020b), resulting in faster advection of saline waters from the open sea to the  
511 Kvarner Bay. Precisely, it was found during the NAdEx experiment (Vilibić et al., 2018) that the  
512 Aladin/HR–ROMS modelling system used by Mihanović et al. (2018) underestimated the  
513 transport from and towards the Kvarner Bay by 50% to even 80%, while the evaluation of the  
514 AdriSC climate model against available *in situ* observations revealed no substantial biases in the  
515 Kvarner Bay (Pranić et al., 2021). Further, previous numerical studies from Denamiel et al.  
516 (2021a) and Pranić et al. (2023) demonstrated that, for proper quantification of the dense water  
517 generation and water exchanges in the Kvarner Bay, both nonhydrostatic atmospheric models  
518 with a maximum resolution of few kilometres and ocean models with at least 1 km resolution  
519 should be used in the Adriatic Sea.

520 The other interesting features of the dense water generation in the Kvarner Bay simulated  
521 with the AdriSC model are that it only contributes ca. 25–35% to the overall dense water mass  
522 outflow and that a smaller secondary peak in PDA is often found during summer, which is  
523 mostly linked to the dynamical behaviour of the deepest Kvarner Bay area as further discussed in  
524 section 4.3.

#### 525 4.2 Adriatic basin vs. Otranto Strait mass transports

526 In the AdriSC historical simulation, the monthly distributions of dense water mass peak  
527 in March across most of the Adriatic basin. This result is aligned with previous observational  
528 studies that demonstrated that the dense waters generated in the northern Adriatic can travel ca.  
529 200 kilometres southward over 2–3 weeks (Vilibić and Mihanović, 2013) and can influence the  
530 thermohaline circulation over the whole Adriatic (Orlić et al., 2007).

531 In contrast with the rest of the Adriatic basin dynamical behaviour, the dense water mass  
532 transported along the western side of the Otranto Strait (transect T8) presents two maxima in  
533 July–August and November–December. The November–December peak is also present along the  
534 full Otranto Strait transect (transect T7) and most likely results from enhanced circulation and  
535 exchange of water masses in the Strait of Otranto. However, the particular behaviour in July–  
536 August is well-illustrated with the animation of the spatial distribution of the PDAs over the  
537 Adriatic Sea (Movie S1) that reveals the presence of dense waters (with PDAs  $>29.4 \text{ kg m}^{-3}$  in  
538 most years) in July–August along the southwestern Adriatic coast which are fast transported  
539 towards the Otranto Strait. This surprising result was never reported in previous observational  
540 studies and needs further investigation to understand whether it is linked to a numerical artefact  
541 within the AdriSC simulation or realistic dynamical features.

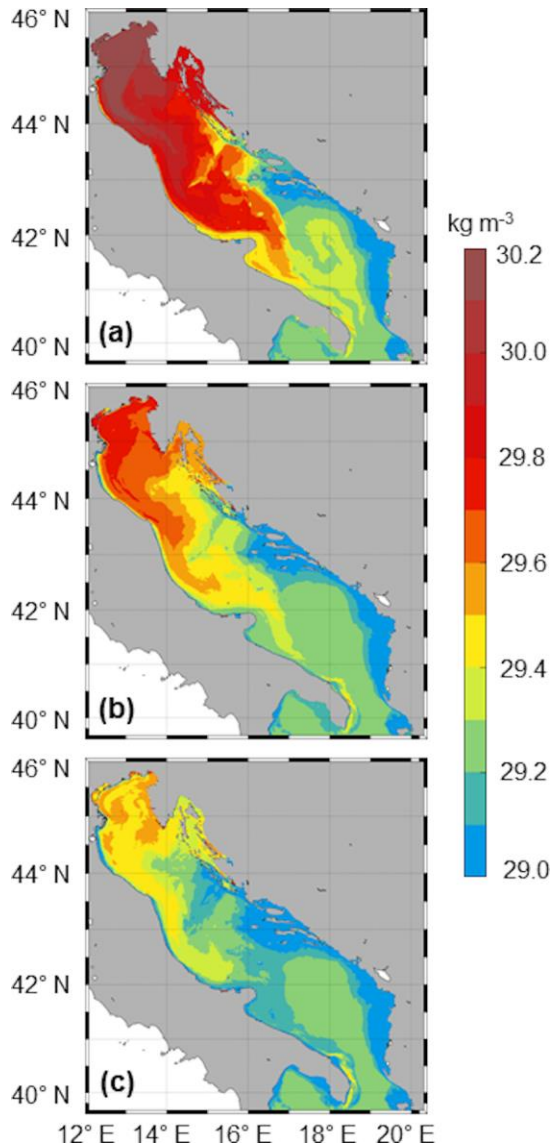
#### 542 4.3 Dynamical behaviour of the accumulation sites

543 The analysis of the AdriSC model highlights that the dense waters accumulated in the  
544 deepest parts of the Kvarner Bay are ventilated annually as the whole bay is regularly mixed  
545 during late autumn and winter, while the dense waters accumulated at the bottom of the Jabuka  
546 Pit and the Southern Adriatic Pit exhibit “saw-tooth” patterns and are renewed every 1–3 years  
547 and every 5–10 years, respectively.

548 First, the dynamical behaviour of the Kvarner Bay as an accumulation site is primarily  
549 linked to its particular geomorphology. Outside of the nearshore areas, most of the depths within  
550 the bay are ranging from 60 to 80 m except for a 110-m pit forming the deep Kvarner Bay  
551 accumulation area (see the domain outreach in Fig. 1). Consequently, weak bottom density  
552 currents are likely to transport the denser waters generated over the shallower regions of the bay  
553 towards this pit. As the differences in depth and density between the pit and the rest of the  
554 Kvarner Bay are small, this transport is also likely to occur for several weeks or even few months  
555 which could explain the presence of a summer peak in the PDA time series extracted over the  
556 full Kvarner Bay subdomain. Additionally, dense waters generated over the open northern  
557 Adriatic shelf are also being spread towards the Kvarner Bay through connecting channels and  
558 may also accumulate in the deepest part of the bay (Vilibić et al., 2018). Second, within the  
559 Jabuka Pit accumulation site, the complete ventilation of the whole water column was previously  
560 reported to rarely occur (e.g., Bergamasco et al., 1999) which explains the “saw-tooth” pattern  
561 simulated with the AdriSC model. Further, new oxygenized waters are almost exclusively  
562 coming from dense waters generated yearly in the northern Adriatic (Nof, 1983; Emms, 1997;  
563 Artegiani and Salusti, 1987). This explains the synchronization of the year-by-year  
564 presence/absence of dense waters within the deep Kvarner Bay and the Jabuka Pit (See Movie  
565 S1). Finally, within the Southern Adriatic Pit, dense waters rarely reach the deepest areas of the  
566 pit and the renewal of the bottom waters seems to follow the BiOS phases. It is more frequent  
567 during the cyclonic BiOS phases (e.g., during the 2000-2006 period as simulated by the AdriSC  
568 model; Denamiel et al., 2022) when the advection of more saline waters from the Ionian Sea  
569 increases the NAddW density but also lower the stability of the water column and, hence,  
570 enhances the AdDW generation (Cardin et al., 2020). In contrast, during the anticyclonic BiOS  
571 phases renewal is almost absent (e.g., during the 2007-2011 period as simulated by the AdriSC  
572 model; Denamiel et al., 2022) indicating that circulation in the northern Ionian Sea is key for the  
573 renewal of the deepest parts of the Adriatic.

#### 574 4.4 Classification of the dense water events

575 A basic classification of the dense water events was derived from the results of maximum  
576 bottom PDA in the northern Adriatic generation site presented in Figure 3, where three  
577 categories were defined for the box plots: strong (median of maximum PDAs  $> 30.0 \text{ kg m}^{-3}$ ),  
578 moderate (median of maximum PDAs  $\geq 29.5 \text{ kg m}^{-3}$  and  $\leq 30.0 \text{ kg m}^{-3}$ ) and weak (median of  
579 maximum PDAs  $< 29.5 \text{ kg m}^{-3}$ ). Spatial distributions of median of the maximum bottom PDAs  
580 in the whole Adriatic for the three categories, are shown on Figure 8.



581  
 582 **Figure 8.** Spatial distribution of median maximum bottom PDA for categories of years with (a)  
 583 strong, (b) moderate, and (c) weak dense water formation, based on the classification of  
 584 maximum PDA in the northern Adriatic during the JFM period (Figure 3).

585 In the first category with strong dense water events (Fig. 8a), maximum PDA values  
 586 surpass  $30.0 \text{ kg m}^{-3}$  in the whole northern Adriatic and reach up to  $30.0 \text{ kg m}^{-3}$  in the Kvarner  
 587 Bay and middle Adriatic. Large PDAs are also present in the Jabuka Pit and along the western  
 588 coast towards the SAP, where an inflow of bottom dense water with PDA up to  $29.4 \text{ kg m}^{-3}$  can  
 589 be noticed, cascading to the bottom SAP layers and forming the near-bottom cyclonic gyre. As  
 590 the near-bottom dense waters need about a month to encircle the SAP (Movie S1), their speed  
 591 may be estimated to ca.  $15 \text{ cm s}^{-1}$  before fully filling the SAP bottom. The second category with  
 592 moderate dense water events (Fig. 8b), is characterized by maximum PDAs up to  $29.8 \text{ kg m}^{-3}$  in  
 593 the northwestern part of the northern Adriatic and up to  $29.7 \text{ kg m}^{-3}$  in the southeastern part of  
 594 the northern Adriatic and along the western side of the middle Adriatic. In the Kvarner Bay, the  
 595 values are mostly between  $29.5$  and  $29.6 \text{ kg m}^{-3}$ , while in the Jabuka Pit they reach up to  $29.5 \text{ kg}$

596  $\text{m}^{-3}$ . Here, an outflow of dense water is still present along the western coast, while the PDA in  
597 the SAP reaches up to  $29.3 \text{ kg m}^{-3}$  with little to no dense water cascading reproduced by the  
598 model. The third category of years with weak dense water formation (Fig. 8c) shows larger  
599 maximum PDAs only in some parts of the northern Adriatic (up to  $29.6 \text{ kg m}^{-3}$ ), while in the  
600 Kvarner Bay and middle Adriatic values mostly reach up to  $29.5 \text{ kg m}^{-3}$ . There is some transport  
601 along the western side of the middle Adriatic, while in the Jabuka Pit and SAP the values are  
602 mostly uniform up to  $29.3 \text{ kg m}^{-3}$  as no dense water cascading occurs in both accumulation sites.

603 The classification of dense water generation events exhibits common spatial patterns in  
604 bottom maximum PDA, while mainly differing in magnitude. To obtain more details on the  
605 similarities and differences in the dense water outflow, additional research should be performed  
606 using not just bottom density data but also currents over the whole water column.

## 607 **5 Conclusions**

608 In this study, the AdriSC climate model has been used to numerically assess, for the very  
609 first time, the Adriatic dense water multi-decadal dynamical properties at 1-km horizontal  
610 resolution. In contrast with previous numerical simulations used in the Adriatic Sea, the  
611 presented results have been demonstrated to be aligned with the known literature mostly relying  
612 on observational studies. Consequently, the AdriSC far-future RCP 8.5 climate simulation (2070-  
613 2100 period) can now be used to assess the impact of extreme climate warming on the Adriatic  
614 thermohaline circulation. An analysis of trends, variability and extreme events based on this  
615 AdriSC far-future simulation (Tojčić et al., 2024) has already demonstrated that the dense water  
616 formation in the northern Adriatic is likely to be reduced while the southern Adriatic cyclonic  
617 gyre is likely to intensify and shrink, and the vertical stratification in the deepest part of the  
618 Adriatic is likely to strengthen. As similar results were also found by Parras-Berrocal et al.  
619 (2023) using one member of the Med-CORDEX ensemble (Ruti et al., 2016), further analyses of  
620 the kilometre-scale atmosphere-ocean AdriSC far-future climate simulation must now be  
621 performed and might provide a new vision of the Adriatic dense water dynamical properties  
622 under extreme warming.

## 623 **Acknowledgments**

624 The computing and archive facilities used in this research were provided by the European Centre  
625 for Medium-range Weather Forecasts (ECMWF) through national quota and the ECMWF  
626 Special Projects ‘The Adriatic decadal and inter-annual oscillations: modelling component’ and  
627 ‘Numerical modelling of the Adriatic-Ionian decadal and inter-annual oscillations: from realistic  
628 simulations to process-oriented experiments’. The research has been supported by the Croatian  
629 Science Foundation projects ADIOS (Grant IP-06-2016-1955), BivACME (Grant IP-2019-04-  
630 8542), C3PO (Grant IP-2022-10-9139) and GLOMETS (Grant IP-2022-10-306), the HORIZON  
631 EUROHPC JU project ChEESE-2P (Grant 101093038), as well as the project of Institute of  
632 Oceanography and Fisheries (Split, Croatia) KLIMADRIA.

633 **Data Availability Statement**

634 The code of the COAWST model as well as the ecFlow pre-processing scripts and the input data  
 635 needed to re-run the AdriSC climate model in evaluation mode can be obtained under the Open  
 636 Science Framework (OSF) data repository (Denamiel, 2021) under the MIT license.  
 637 The model results used to produce this article can be obtained under the Open Science  
 638 Framework (OSF) FAIR data repository (Pranić, 2024).

639 **References**

640 Artegiani, A. & Salusti, E. (1987), Field observation of the flow of dense water on the bottom of  
 641 the Adriatic Sea during the winter of 1981. *Oceanologica Acta*, 10, 387-391.

642 Artegiani, A., Bregant, D., Paschini, E., Pinardi, N., Raicich, F., & Russo, A. (1997), The  
 643 Adriatic Sea general circulation, part I: air-sea interactions and water mass structure, *Journal of*  
 644 *Physical Oceanography*, 27, 1492–1514. [doi:10.1175/1520-](https://doi.org/10.1175/1520-0485(1997)027<1492:TASGCP>2.0.CO;2)  
 645 [0485\(1997\)027<1492:TASGCP>2.0.CO;2](https://doi.org/10.1175/1520-0485(1997)027<1492:TASGCP>2.0.CO;2)

646 Artegiani, A., Marini, M., Pariante, R., Paschini, E., & Russo, A. (2001), Evolution of physical  
 647 parameters and chemical observations in the Middle Adriatic depressions. *Archo Oceanography*  
 648 *Limnology*, 22, 27-34.

649 Batistić, M., Garić, R., & Molinero, J.C. (2004), Interannual variations in Adriatic Sea  
 650 zooplankton mirror shifts in circulation regimes in the Ionian Sea. *Climate Research*, 61, 231-  
 651 240. [doi:10.3354/cr01248](https://doi.org/10.3354/cr01248)

652 Belušić, D., & Klaić, Z. B. (2004), Estimation of bora wind gusts using a limited area model.  
 653 *Tellus*, 56, 296–307, doi:10.1111/j.1600-0870.2004.00068.x

654 Bensi, M., Cardin, V., Rubino, A., Notarstefano, G., & Poulain, P.M. (2013), Effects of winter  
 655 convection on the deep layer of the Southern Adriatic Sea in 2012. *Journal of Geophysical*  
 656 *Research: Oceans*, 118, 6064-6075, [doi:10.1002/2013JC009432](https://doi.org/10.1002/2013JC009432)

657 Bergamasco, A., Oguz, T., & Malanotte-Rizzoli, P. (1999), Modeling dense water mass  
 658 formation and winter circulation in the northern and central Adriatic Sea. *J. Mar. Syst.*, 20, 279–  
 659 300. [doi:10.1016/S0924-7963\(98\)00087-6](https://doi.org/10.1016/S0924-7963(98)00087-6)

660 Boldrin, A., Carniel, S., Giani, M., Marini, M., Bernardi Aubry, F., Campanelli, A., Grilli, F., &  
 661 Russo, A. (2009), Effects of bora wind on physical and biogeochemical properties of stratified  
 662 waters in the northern Adriatic. *Journal of Geophysical Research*, 114, C08S92,  
 663 [doi:10.1029/2008JC004837](https://doi.org/10.1029/2008JC004837)

664 Bowman, A. W., & Azzalini, A. (1997), *Applied Smoothing Techniques for Data Analysis*. New  
 665 York: Oxford University Press Inc., ISBN 0191545694.

666 Cardin, V., Wirth, A., Khosravi, M., & Gačić, M. (2020), South Adriatic recipes: Estimating the  
 667 vertical mixing in the deep pit. *Frontiers in Marine Science*, 7, 565982,  
 668 [doi:10.3389/fmars.2020.565982](https://doi.org/10.3389/fmars.2020.565982)

- 669 Civitarese, G., Gačić, M., Batistić, M., Bensi, M., Cardin, V., Dulčić, J., Garić, R., & Menna, M.  
670 (2023), The BiOS mechanism: History, theory, implications. *Progress in Oceanography*, 216,  
671 103056. [doi:10.1016/j.pocean.2023.103056](https://doi.org/10.1016/j.pocean.2023.103056)
- 672 Denamiel, C. L. (2021), AdriSC Climate Model: Evaluation Run. OSF [code],  
673 [doi:10.17605/OSF.IO/ZB3CM](https://doi.org/10.17605/OSF.IO/ZB3CM)
- 674 Denamiel, C., Šepić, J., Ivanković, D., & Vilibić, I. (2019), The Adriatic Sea and Coast  
675 modelling suite: Evaluation of the meteotsunami forecast component. *Ocean Modelling*, 135,  
676 71–93. [doi:10.1016/j.ocemod.2019.02.003](https://doi.org/10.1016/j.ocemod.2019.02.003)
- 677 Denamiel, C., Tojčić, I., & Vilibić, I. (2020a), Far future climate (2060–2100) of the northern  
678 Adriatic air–sea heat transfers associated with extreme bora events. *Climate Dynamics*, 55,  
679 3043–3066. [doi:10.1007/s00382-020-05435-8](https://doi.org/10.1007/s00382-020-05435-8)
- 680 Denamiel, C., Pranić, P., Quentin, F., Mihanović, H., & Vilibić, I. (2020b), Pseudo-global  
681 warming projections of extreme wave storms in complex coastal regions: The case of the  
682 Adriatic Sea. *Climate Dynamics*, 55, 2483–2509. [doi:10.1007/s00382-020-05397-x](https://doi.org/10.1007/s00382-020-05397-x)
- 683 Denamiel, C., Tojčić, I., & Vilibić, I. (2021a), Balancing accuracy and efficiency of atmospheric  
684 models in the northern Adriatic during severe bora events. *Journal of Geophysical Research:*  
685 *Oceans*, 126, e2020JD033516. [doi:10.1029/2020JD033516](https://doi.org/10.1029/2020JD033516)
- 686 Denamiel, C., Pranić, P., Ivanković, D., Tojčić, I., & Vilibić, I. (2021b), Performance of the  
687 Adriatic Sea and Coast (AdriSC) climate component—a COAWST V3.3-based coupled  
688 atmosphere-ocean modelling suite: atmospheric dataset. *Geoscientific Model Development*, 14,  
689 3995–4017. [doi:10.5194/gmd-14-3995-202127](https://doi.org/10.5194/gmd-14-3995-202127)
- 690 Denamiel, C., Tojčić, I., Pranić, P., & Vilibić, I. (2022), Modes of the BiOS-driven Adriatic Sea  
691 thermohaline variability. *Climate Dynamics*, 59, 1097–1113, [doi:10.1007/s00382-022-06178-4](https://doi.org/10.1007/s00382-022-06178-4)
- 692 Dorman, C. E., Carniel, S., Cavaleri, L., Sclavo, M., Chiggiato, J., Doyle, J., Haack, T., Pullen,  
693 J., Grbec, B., Vilibić, I., Janeković, I., Lee, C., Malačić, V., Orlić, M., Paschini, E., Russo, A.,  
694 & Signell, R. P. (2007), Winter 2003 marine atmospheric conditions and the bora over the  
695 northern Adriatic. *Journal of Geophysical Research: Oceans*, 112, C03S03.  
696 [doi:10.1029/2005JC003134](https://doi.org/10.1029/2005JC003134)
- 697 Dukowicz, J. K. (2001), Reduction of pressure and pressure gradient errors in ocean simulations.  
698 *Journal of Physical Oceanography*, 31, 1915–1921. [doi:10.1175/1520-  
699 0485\(2001\)031<1915:RODAPG>2.0.CO;2](https://doi.org/10.1175/1520-0485(2001)031<1915:RODAPG>2.0.CO;2)
- 700 Dunić, N., Vilibić, I., Šepić, J., Mihanović, H., Sevault, F., Somot, S., Waldman, R., Nabat, P.,  
701 Arsouze, T., Pennel, R., Jordà, J., & Precali, R. (2019), Performance of multi-decadal ocean  
702 simulations in the Adriatic Sea. *Ocean Modelling*, 134, 84–109.  
703 [doi:10.1016/j.ocemod.2019.01.006](https://doi.org/10.1016/j.ocemod.2019.01.006)
- 704 Emms, P.W. (1997), Streamtube models of gravity currents in the ocean. *Deep-Sea Research I*,  
705 44, 1575–1610. [doi:10.1016/S0967-0637\(97\)00047-2](https://doi.org/10.1016/S0967-0637(97)00047-2)

- 706 Foglini, F., Campiani, E., & Trincardi, F. (2016), The reshaping of the South West Adriatic  
707 Margin by cascading of dense shelf waters, *Marine Geology.*, 375, 64–81.  
708 [doi:10.1016/j.margeo.2015.08.011](https://doi.org/10.1016/j.margeo.2015.08.011)
- 709 Gačić, M., Civitarese, G., Miserocchi, S., Cardin, V., Crise, A., & Mauri, E. (2002), The open-  
710 ocean convection in the Southern Adriatic: a controlling mechanism of the spring phytoplankton  
711 bloom. *Continental Shelf Research*, 22, 1897-1908. [doi:10.1016/S0278-4343](https://doi.org/10.1016/S0278-4343)
- 712 Gačić, M., Borzelli, G. E., Civitarese, G., Cardin, V., & Yari, S. (2010), Can internal processes  
713 sustain reversals of the ocean upper circulation? The Ionian Sea example. *Geophysical Research*  
714 *Letters*, 37(9). [doi:10.1029/2010GL043216](https://doi.org/10.1029/2010GL043216)
- 715 Gačić, M., Civitarese, G., Kovačević, V., Ursella, L., Bensi, M., Menna, M., Cardin, V., Poulain,  
716 P.-M., Cosoli, S., Notarstefano, G., & Pizzi, C. (2014), Extreme winter 2012 in the Adriatic: an  
717 example of climatic effect on the BiOS rhythm. *Ocean Science*, 10, 513–522. [doi:10.5194/os-10-](https://doi.org/10.5194/os-10-513-2014)  
718 [513-2014](https://doi.org/10.5194/os-10-513-2014)
- 719 Janeković, I., Mihanović, H., Vilibić, I., & Tudor, M. (2014), Extreme cooling and dense water  
720 formation estimates in open and coastal regions of the Adriatic Sea during the winter of 2012. *J.*  
721 *Geophysical Research: Oceans*, 119, 3200–3218. [doi:10.1002/ 2014JC009865](https://doi.org/10.1002/2014JC009865)
- 722 Jasprica, N., Čalić, M., Kovačević, V., Bensi, M., Dupčić Radić, I., Garić, R., & Batistić, M.  
723 (2022), Phytoplankton distribution related to different winter conditions in 2016 and 2017 in the  
724 open southern Adriatic Sea (eastern Mediterranean). *Journal of Marine Systems*, 226, 103665.  
725 [doi:10.1016/j.jmarsys.2021.103665](https://doi.org/10.1016/j.jmarsys.2021.103665)
- 726 Laprise, R. (1992), The Euler Equations of motion with hydrostatic pressure as independent  
727 variable, *Monthly Weather Reviews*, 120, 197–207. [doi:10.1175/1520-](https://doi.org/10.1175/1520-0493(1992)120<0197:TEEOMW>2.0.CO;2)  
728 [0493\(1992\)120<0197:TEEOMW>2.0.CO;2.](https://doi.org/10.1175/1520-0493(1992)120<0197:TEEOMW>2.0.CO;2)
- 729 Langone, L., Conese, I., Miserocchi, S., Boldrin, A., Bonaldo, D., Carniel, S., Chiggiato, J.,  
730 Turchetto, M., Borghini, M., & Tesi, T. (2016), Dynamics of particles along the western margin  
731 of the Southern Adriatic: Processes involved in transferring particulate matter to the deep basin.  
732 *Marine Geology*, 375, 28–43. [doi:10.1016/j.margeo.2015.09.004](https://doi.org/10.1016/j.margeo.2015.09.004)
- 733 Levitus, S., & Boyer, T.P. (1994a), *World Ocean Atlas 1994, Volume 4: Temperature*, NOAA  
734 Atlas NESDIS 4, US Dept. of Commerce.
- 735 Levitus, S., Burgett, R., & Boyer, T.P. (1994b), *World Ocean Atlas 1994, Volume 3: Salinity*,  
736 NOAA Atlas NESDIS 3, US Dept. Commerce.
- 737 Ličer, M., Smerkol, P., Fettich, A., Ravdas, M., Papapostolou, A., Mantziafou, A., Strajnar, B.,  
738 Cedilnik, J., Jeromel, M., Jerman, J., Petan, S., Malačič, V., & Sofianos, S. (2016), Modeling the  
739 ocean and atmosphere during an extreme bora event in northern Adriatic using one-way and two-  
740 way atmosphere–ocean coupling. *Ocean Science*, 12, 71-86. [doi:10.5194/os-12-71-2016](https://doi.org/10.5194/os-12-71-2016)

- 741 Mantziafou, A., & Lascaratos, A. (2008), Deep-water formation in the Adriatic Sea: interannual  
742 simulations for the years 1979–1999. *Deep–Sea Research I*, 55, 1403–1427.  
743 [doi:10.1016/j.dsr.2008.06.005](https://doi.org/10.1016/j.dsr.2008.06.005)
- 744 Mihanović, H., Vilibić, I., Carniel, S., Tudor, M., Russo, A., Bergamasco, A., Bubić, N.,  
745 Ljubešić, Z., Viličić, D., Boldrin, A., Malačić, V., Celio, M., Comici, C., & Raicich, F. (2013),  
746 Exceptional dense water formation on the Adriatic shelf in the winter of 2012. *Ocean Science*, 9,  
747 561–572. [doi:10.5194/os-9-561-2013](https://doi.org/10.5194/os-9-561-2013)
- 748 Mihanović, H., Janeković, I., Vilibić, Bensi, M., & Kovačević, V. (2018), Modelling interannual  
749 changes in dense water formation on the northern Adriatic shelf. *Pure and Appl. Geophysics*,  
750 175, 4065–4081. [doi:10.1007/s00024-018-1935-5](https://doi.org/10.1007/s00024-018-1935-5)
- 751 Mihanović, H., Vilibić, I., Šepić, J., Matić, F., Ljubešić, Z., Mauri, E., Gerin, R., Notarstefano,  
752 G., & Poulain, P.-M. (2021), Observation, preconditioning and recurrence of exceptionally high  
753 salinities in the Adriatic Sea. *Frontiers in Marine Science*, 8, 672210.  
754 [doi:10.3389/fmars.2021.672210](https://doi.org/10.3389/fmars.2021.672210)
- 755 Nof, D. (1983), The translation of isolated cold eddies along a sloping bottom. *Deep-Sea*  
756 *Research*, 30, 171–182. [doi:10.1016/0198-0149\(83\)90067-5](https://doi.org/10.1016/0198-0149(83)90067-5)
- 757 Oddo, P., & Guarnieri, A. (2011), A study of the hydrographic conditions in the Adriatic Sea  
758 from numerical modelling and direct observations (2000–2008). *Ocean Science*, 7, 549–567,  
759 [doi:10.5194/os-7-549-2011](https://doi.org/10.5194/os-7-549-2011)
- 760 Orlić, M., Dadić, V., Grbec, B., Leder, N., Marki, A., Matić, F., Mihanović, H., Beg Paklar, G.,  
761 Pasarić, M., Pasarić, Z., & Vilibić, I. (2007), Wintertime buoyancy forcing, changing seawater  
762 properties and two different circulation systems produced in the Adriatic. *Journal of Geophysical*  
763 *Research: Oceans*, 112, C03S07. [doi:10.1029/2005JC003271](https://doi.org/10.1029/2005JC003271)
- 764 Paladini de Mendoza, F., Schroeder, K., Langone, L., Chiggiato, J., Borghini, M., Giordano, P.,  
765 Verazzo, G., Miserocchi, S. (2022), Deep-water hydrodynamic observations of two moorings  
766 sites on the continental slope of the southern Adriatic Sea (Mediterranean Sea). *Earth System*  
767 *Science Data*, 14, 5617–5635. [doi:10.5194/essd-14-5617-2022](https://doi.org/10.5194/essd-14-5617-2022)
- 768 Parras-Berrocal, I. M., Vázquez, R., Cabos, W., Sein, D. V., Álvarez, O., Bruno, M., &  
769 Izquierdo, A. (2023), Dense water formation in the eastern Mediterranean under a global  
770 warming scenario. *Ocean Science*, 19, 941–952. [doi:10.5194/os-19-941-2023](https://doi.org/10.5194/os-19-941-2023)
- 771 Pranić, P. (2024), Kilometre-Scale Climatology of the Adriatic Dense Water. OSF [dataset].
- 772 Pranić, P., Denamiel, C., & Vilibić, I. (2021), Performance of the Adriatic Sea and Coast  
773 (AdriSC) climate component—a COAWST V3.3-based one-way coupled atmosphere–ocean  
774 modelling suite: ocean results. *Geoscientific Model Development*, 14, 5927–5955.  
775 [doi:10.5194/gmd-14-5927-2021](https://doi.org/10.5194/gmd-14-5927-2021)
- 776 Pranić, P., Denamiel, C., Janeković, I., & Vilibić, I. (2023), Multi-model analysis of Adriatic  
777 dense-water dynamics. *Ocean Science*, 19, 649–670. [doi:10.5194/os-19-649-2023](https://doi.org/10.5194/os-19-649-2023)

- 778 Querin, S., Bensi, M., Cardin, V., Solidoro, C., Bacer, S., Mariotti, L., Stel, F., & Malačić, V.  
779 (2016), Saw-tooth modulation of the deep-water thermohaline properties in the southern Adriatic  
780 Sea. *J. Geophys. Res. Oceans*, 121, 4585–4600. [doi:10.1002/2015JC011522](https://doi.org/10.1002/2015JC011522)
- 781 Raicich, F., Malačić, V., Celio, M., Gaiotti, D., Cantoni, C., Colucci, R.R., Čermelj, B., &  
782 Pucillo, A. (2013), Extreme air–sea interactions in the Gulf of Trieste (North Adriatic) during the  
783 strong Bora event in winter 2012. *Journal of Geophysical Research*, 118, 5238–5250,  
784 [doi:10.1002/jgrc.20398](https://doi.org/10.1002/jgrc.20398)
- 785 Roether, W., Klein, B., Manca, B.B., Theocharis, A., Kioroglou, S. (2007), Transient Eastern  
786 Mediterranean deep waters in response to the massive dense-water output of the Aegean Sea in  
787 the 1990’s. *Progress in Oceanography* 74:540–571, [doi:10.1016/j.pocean.2007.03.001](https://doi.org/10.1016/j.pocean.2007.03.001)
- 788 Ruti, P., Somot, S., Giorgi, F., Dubois, C., Flaounas, E., Obermann, A., et al. (2016), Med-  
789 CORDEX initiative for Mediterranean climate studies. *Bulletin of American Meteorological*  
790 *Society*, 97, 1187–1208. [doi:10.1175/BAMS-D-14-00176.1](https://doi.org/10.1175/BAMS-D-14-00176.1)
- 791 Shchepetkin, A.F., & McWilliams, J.C. (2009), Correction and commentary for “Ocean  
792 forecasting in terrain-following coordinates: Formulation and skill assessment of the regional  
793 ocean modeling system” by Haidvogel et al., *Journal of Computational Physics*, 227, pp. 3595–  
794 3624, *Journal of Computational Physics* 228, 8985–9000. [doi:10.1016/j.jcp.2009.09.002](https://doi.org/10.1016/j.jcp.2009.09.002)
- 795 Skamarock, W. C., Klemp, J. B., Dudhia, J., Gill, D. O., Barker, D. M., Wang, W., & Powers, J.  
796 G. (2005), A description of the Advanced Research WRF Version 2, NCAR Technical Note  
797 NCAR/TN468+STR, [doi:10.5065/D6DZ069T](https://doi.org/10.5065/D6DZ069T)
- 798 Tojčić, I., Denamiel, C., & Vilibić, I. (2023), Kilometer-scale trends and variability of the  
799 Adriatic present climate (1987–2017). *Climate Dynamics*, 61, 2521–2545. [doi:10.1007/s00382-](https://doi.org/10.1007/s00382-023-06700-2)  
800 [023-06700-2](https://doi.org/10.1007/s00382-023-06700-2)
- 801 Tojčić, I., Denamiel, C., & Vilibić, I. (2024), Kilometer-scale trends, variability, and extremes of  
802 the Adriatic far-future climate (RCP 8.5, 2070–2100). *Frontiers in Marine Science*, 11, 1329020.  
803 [doi:fmars.2024.1329020](https://doi.org/10.3389/fmars.2024.1329020)
- 804 Vilibić, I. & Orlić, M. (2001), Least squares tracer analysis of water masses in the South Adriatic  
805 (1967–1990). *Deep-Sea Research I*, 48, 2297–2330. [doi:10.1016/S0967-0637\(01\)00014-0](https://doi.org/10.1016/S0967-0637(01)00014-0)
- 806 Vilibić, I., & Orlić, M. (2002), Adriatic water masses, their rates of formation and transport  
807 through the Otranto Strait. *Deep-Sea Research I*, 49, 1321–1340. [doi:10.1016/S0967-](https://doi.org/10.1016/S0967-0637(02)00028-6)  
808 [0637\(02\)00028-6](https://doi.org/10.1016/S0967-0637(02)00028-6)
- 809 Vilibić, I. Grbec, B., & Supić, N. (2004), Dense water generation in the north Adriatic in 1999  
810 and its recirculation along the Jabuka Pit. *Deep-Sea Research I*, 51, 1457–1474.  
811 [doi:10.1016/j.dsr.2004.07.012](https://doi.org/10.1016/j.dsr.2004.07.012)
- 812 Vilibić, I., Beg Paklar, G., Žagar, N., Mihanović, H., Supić, N., Žagar, M., Domijan, N., &  
813 Pasarić, M. (2008), Summer breakout of trapped bottom dense water from the northern Adriatic.  
814 *Journal of Geophysical Research: Oceans*, 113, C11S02. [doi:10.1029/2007JC004535](https://doi.org/10.1029/2007JC004535)

- 815 Vilibić, I., & Mihanović, H. (2015), Observing the bottom density current over a shelf using an  
816 Argo profiling float. *Geophysical Research Letters*, 40, 910–915, [doi:10.1002/grl.50215](https://doi.org/10.1002/grl.50215)
- 817 Vilibić, I., Mihanović, H., Janeković, I., Denamiel, C., Poulain, P.-M., Orlić, M., Dunić, N.,  
818 Dadić, V., Pasarić, M., Muslim, S., Gerin, R., Matic, F., Šepić, J., Mauri, E., Kokkini, Z., Tudor,  
819 M., Kovač, Ž., & Džoić, T. (2018), Wintertime dynamics in the coastal northeastern Adriatic  
820 Sea: the NAdEx 2015 experiment. *Ocean Science*, 14. [doi:10.5194/os-14-237-2018](https://doi.org/10.5194/os-14-237-2018), 237-258
- 821 Vilibić, I., Pranić, P., & Denamiel, C. (2023), North Adriatic Dense Water: lessons learned since  
822 the pioneering work of Mira Zore-Armanda 60 years ago. *Acta Adriatica*, 38, 100527.  
823 [doi:10.32582/aa.64.1.11](https://doi.org/10.32582/aa.64.1.11)
- 824 Viličić, D., Kuzmić, M., Bosak, S., Šilović, T., Hrustić, E., & Burić, Z. (2009), Distribution of  
825 phytoplankton along the thermohaline gradient in the north-eastern Adriatic channel; winter  
826 aspect. *Oceanologia*, 51, 495-513. [doi:10.5697/oc.51-4.495](https://doi.org/10.5697/oc.51-4.495)
- 827 Warner, J. C., Armstrong, B., He, R., & Zambon, J. B. (2010), Development of a Coupled  
828 Ocean-Atmosphere-Wave-Sediment Transport (COAWST) modeling system. *Ocean Modelling*,  
829 35, 230–244. [doi :10.1016/j.ocemod.2010.07.010](https://doi.org/10.1016/j.ocemod.2010.07.010)
- 830 Zore-Armanda, M. (1963), Les masses d'eau de la mer Adriatique. *Acta Adriatica*, 10, 5–88.

Figure 1.

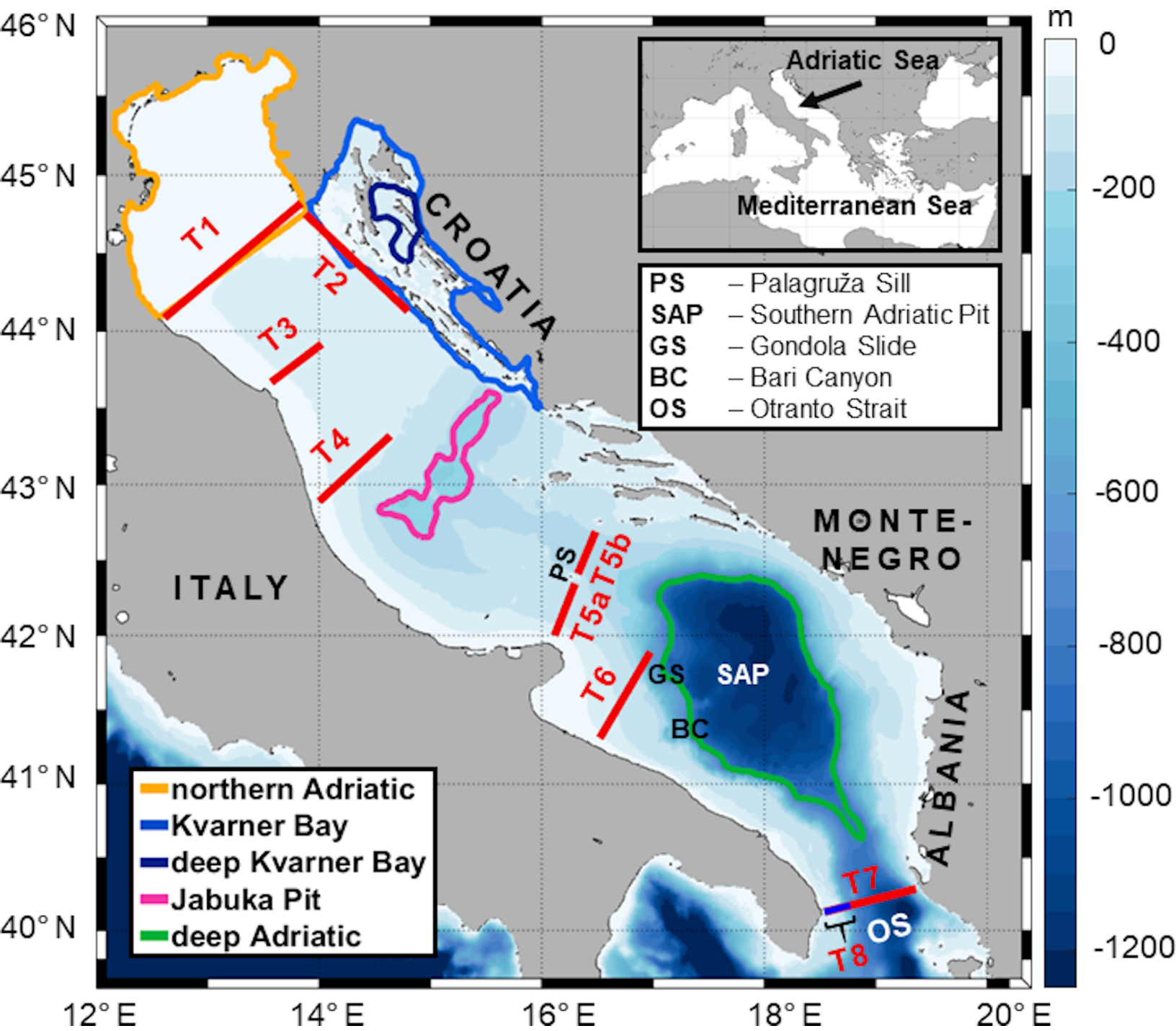


Figure 2.

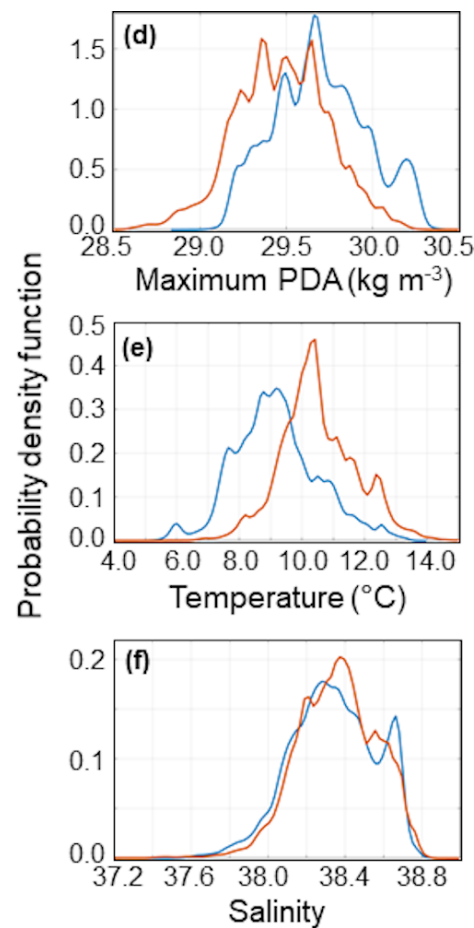
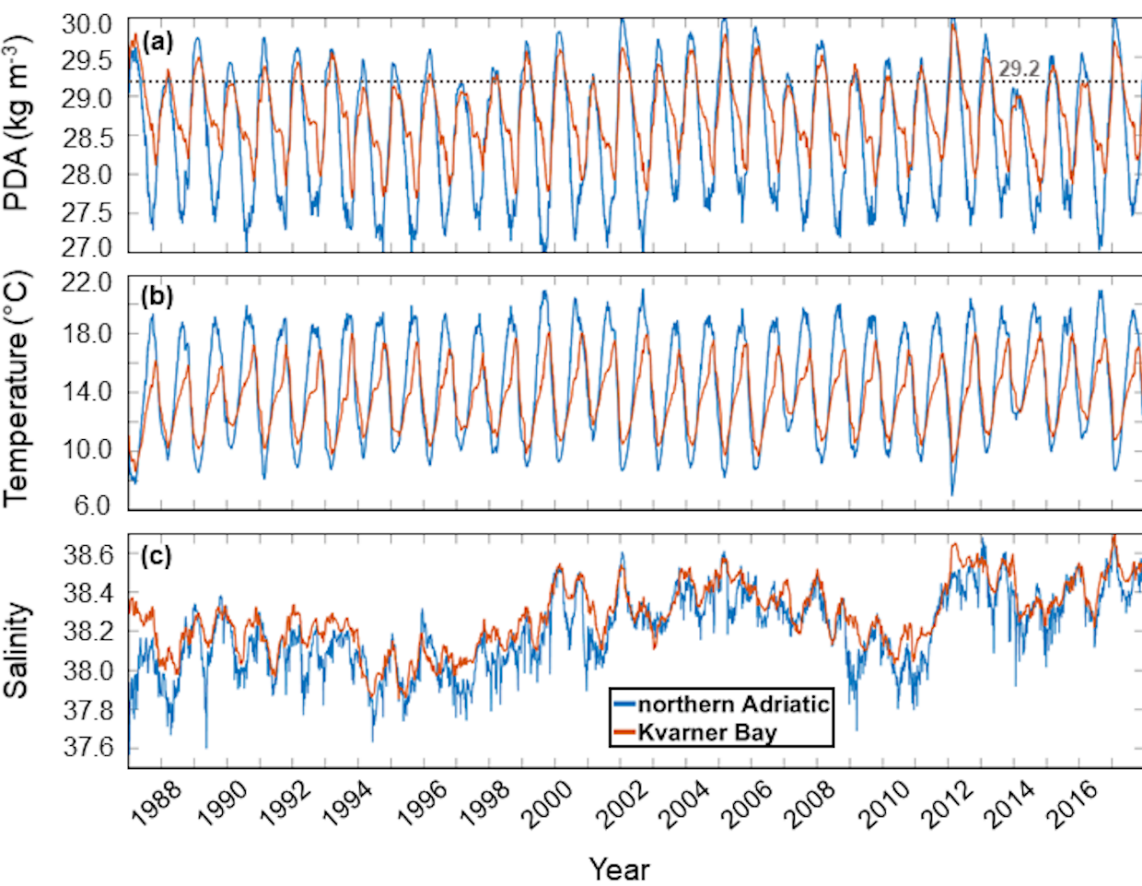


Figure 3.

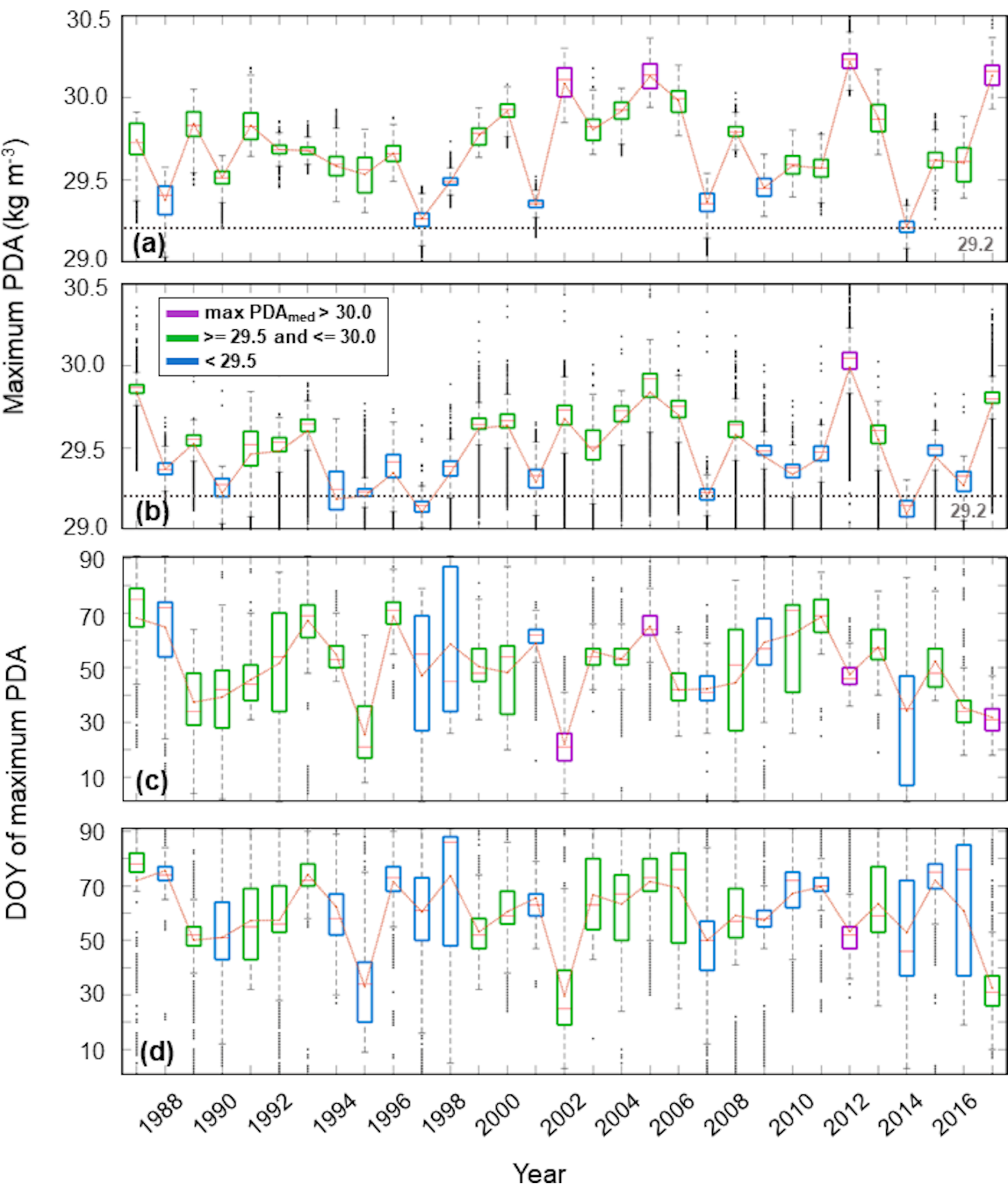


Figure 4.

Monthly bottom dense-water mass transported outward ( $10^{11}$  kg)

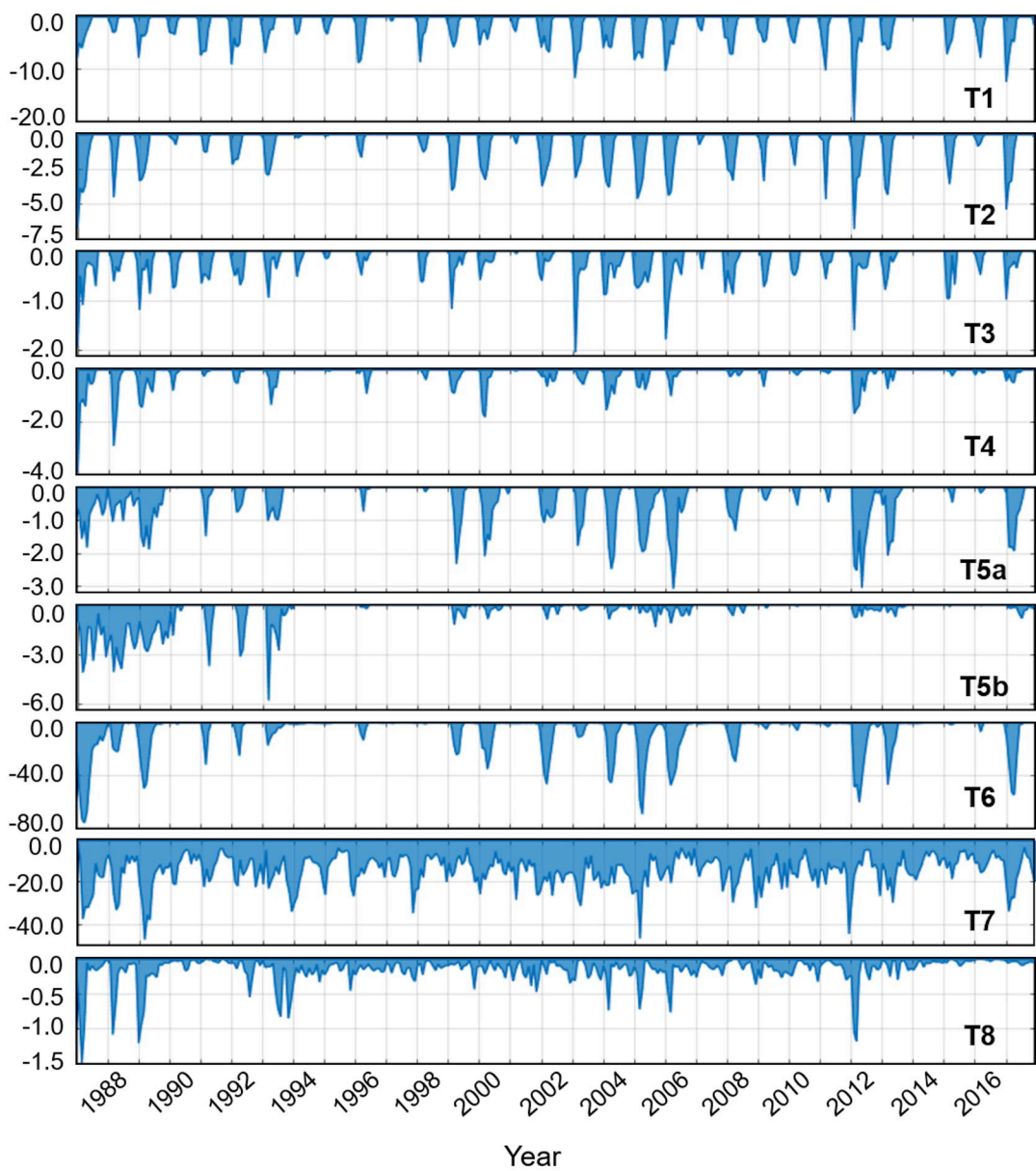


Figure 5.

Climatology of monthly bottom dense-water mass transported outward ( $10^{11}$  kg)

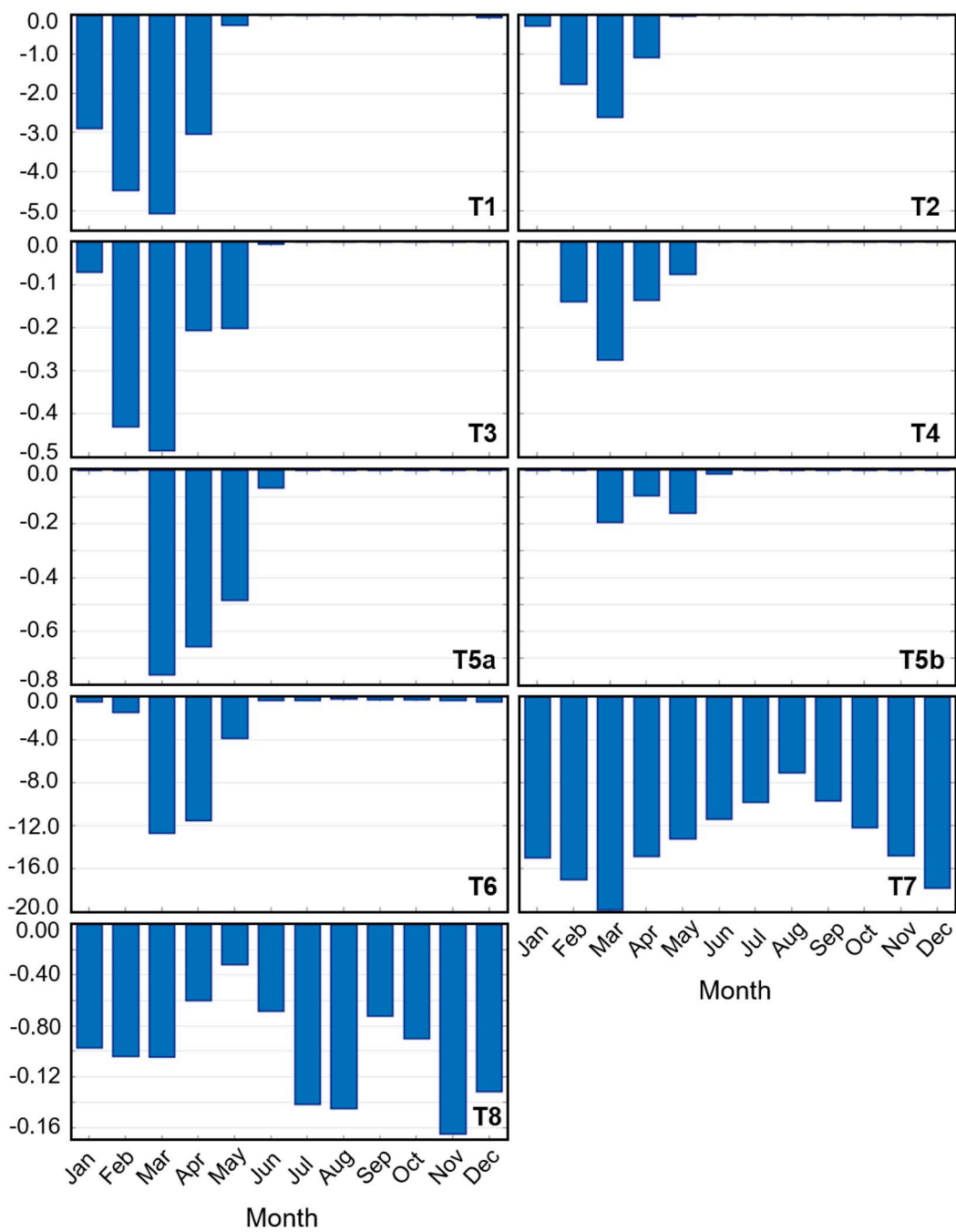


Figure 6.

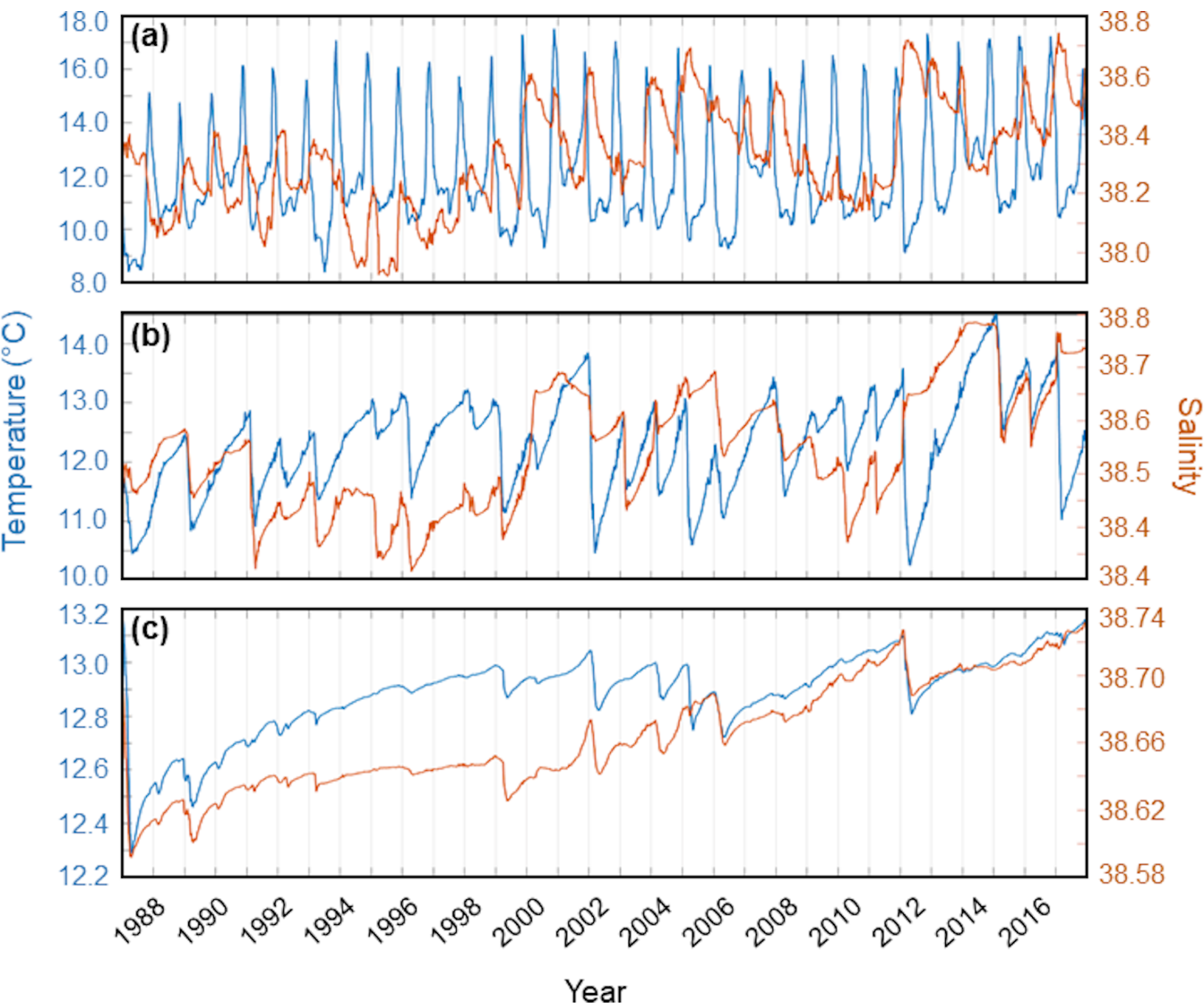


Figure 7.

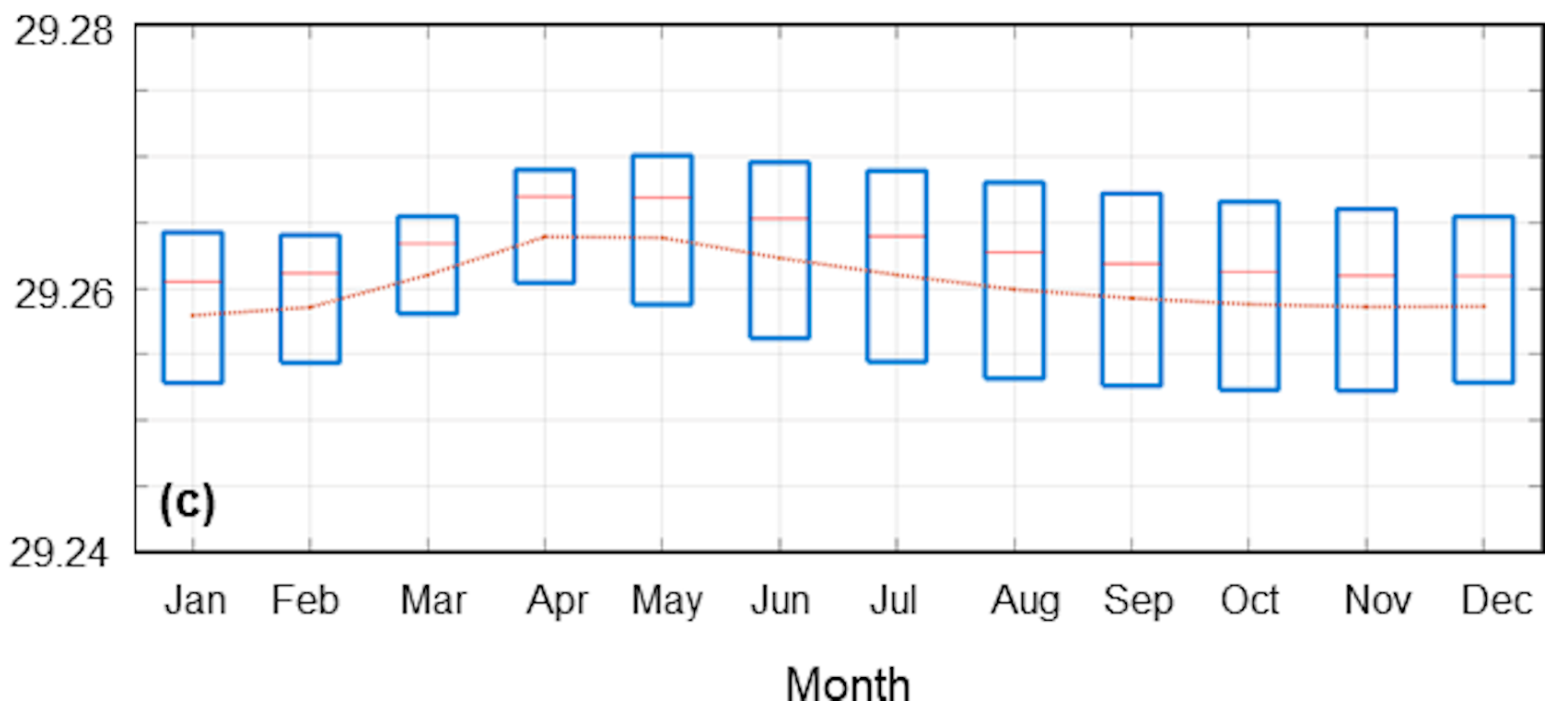
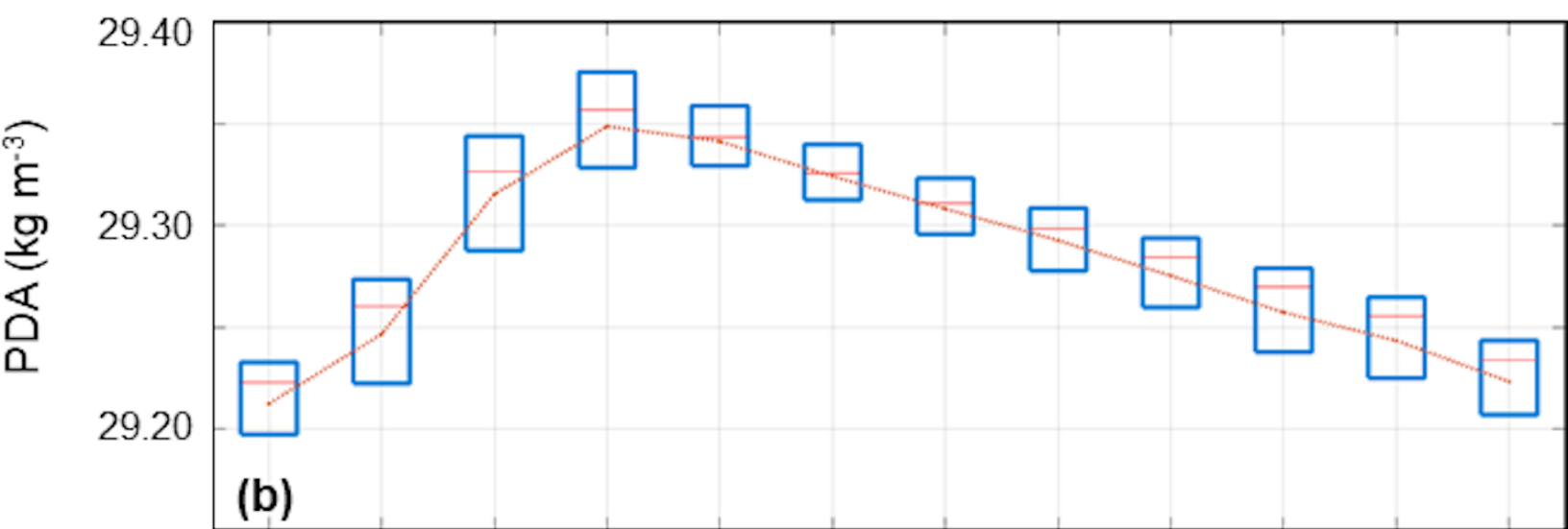
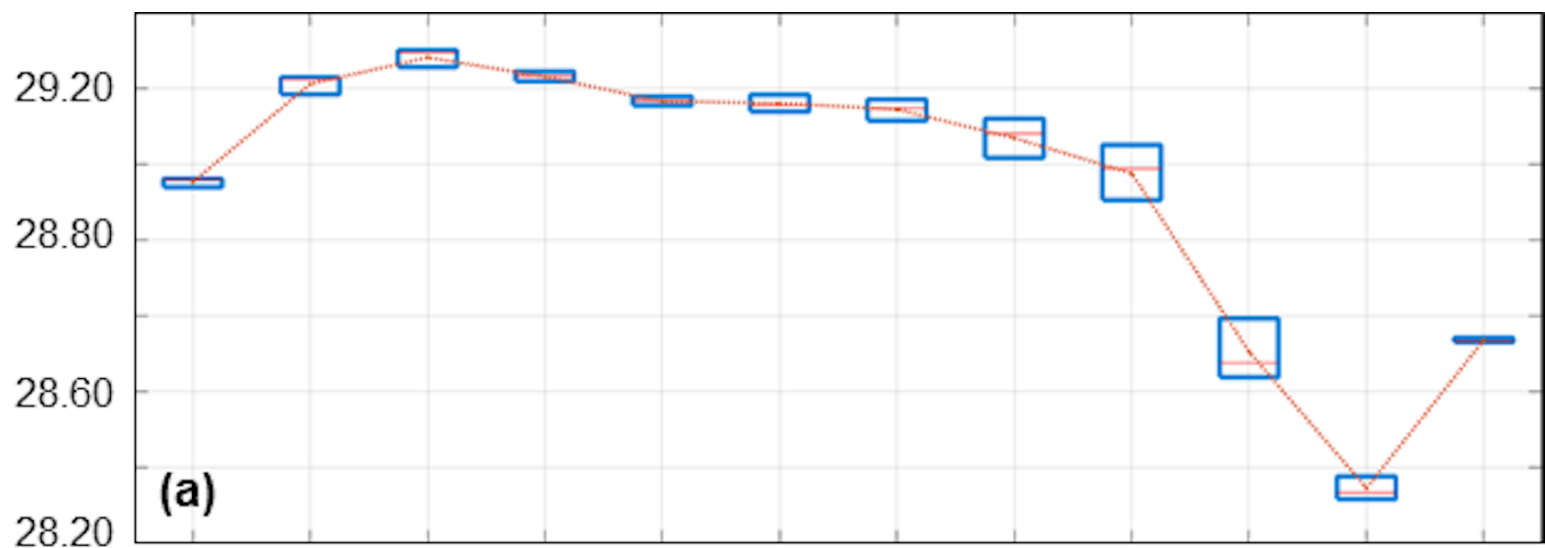


Figure 8.

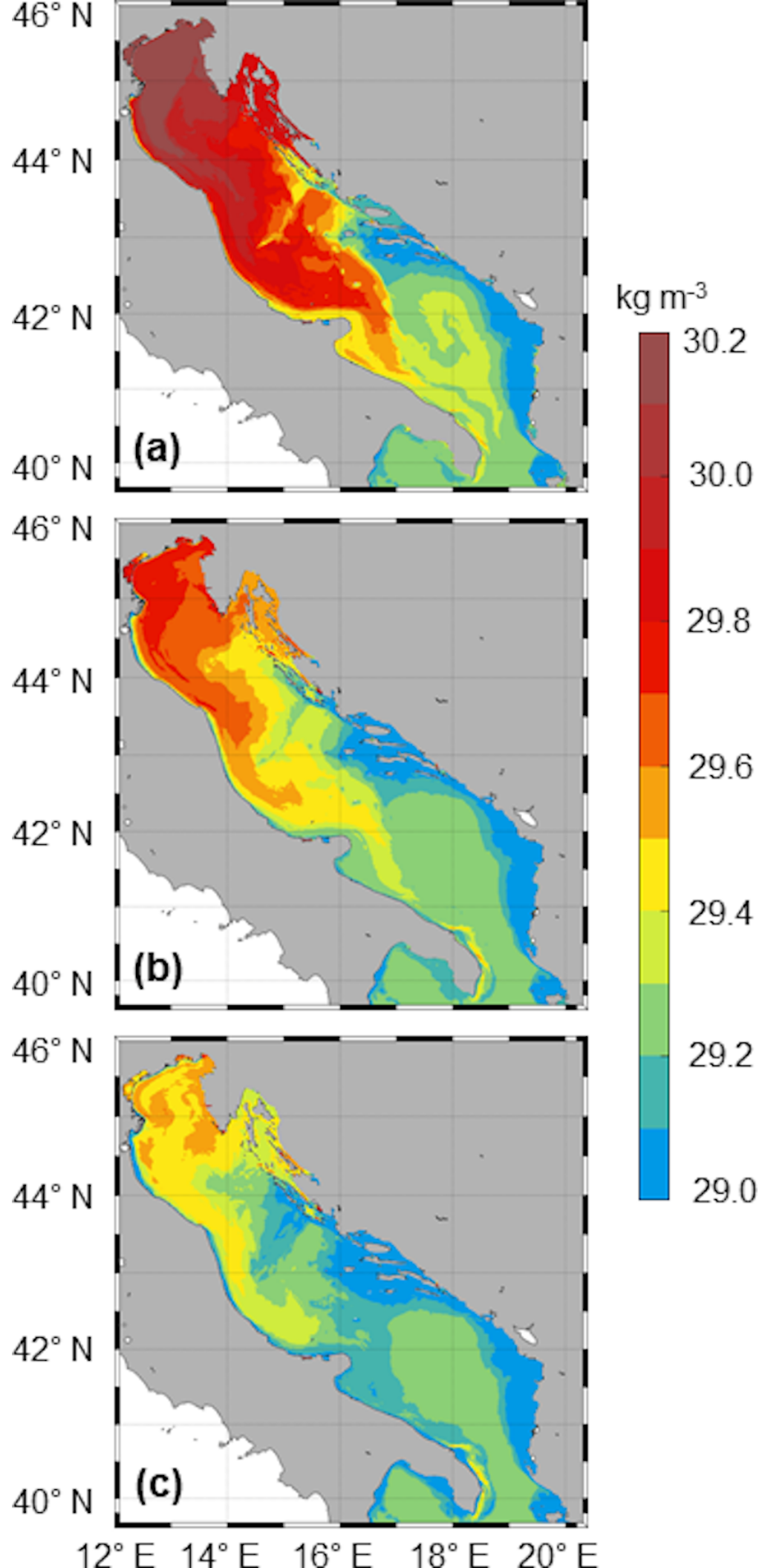


Figure S1.

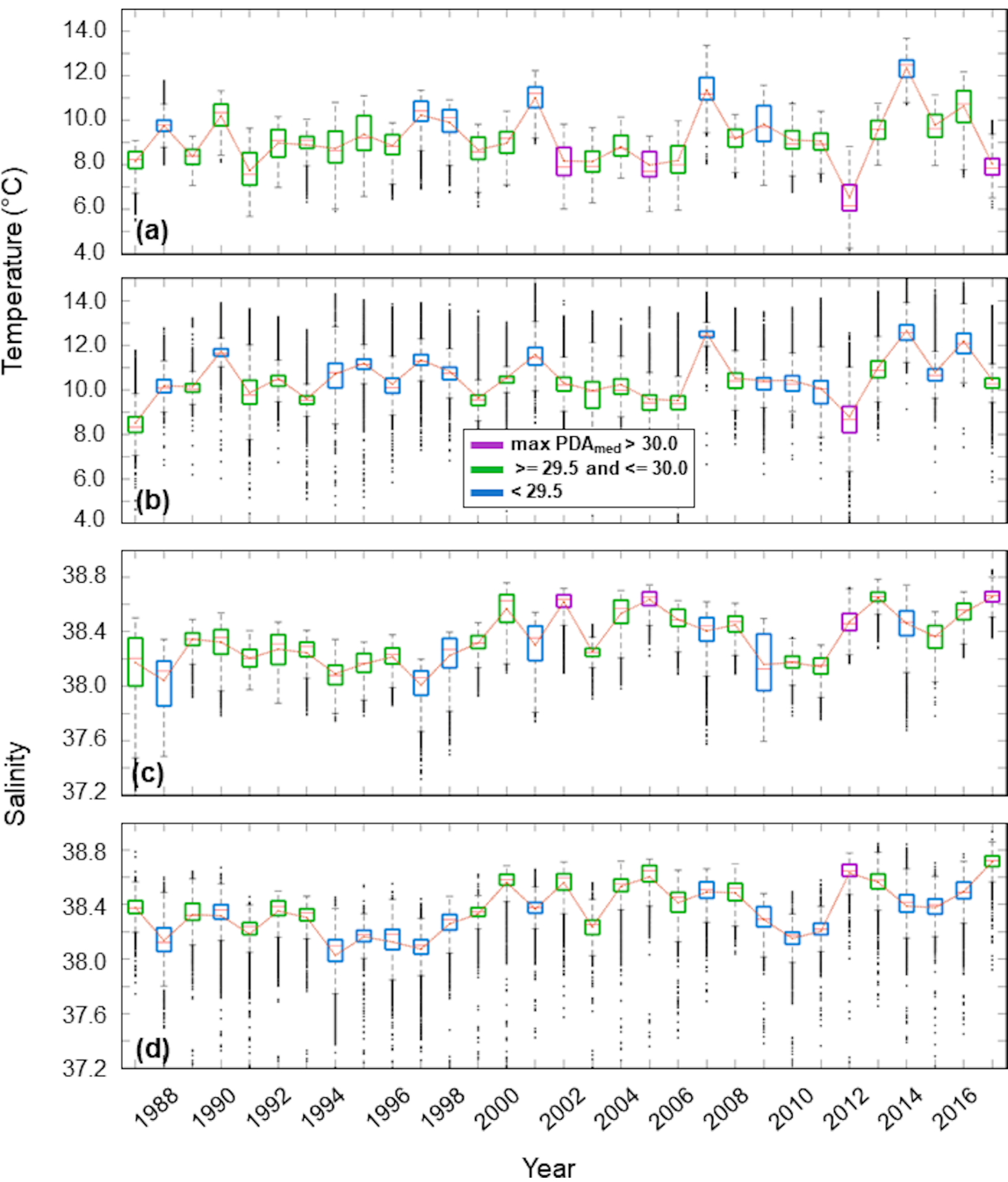


Figure S2.

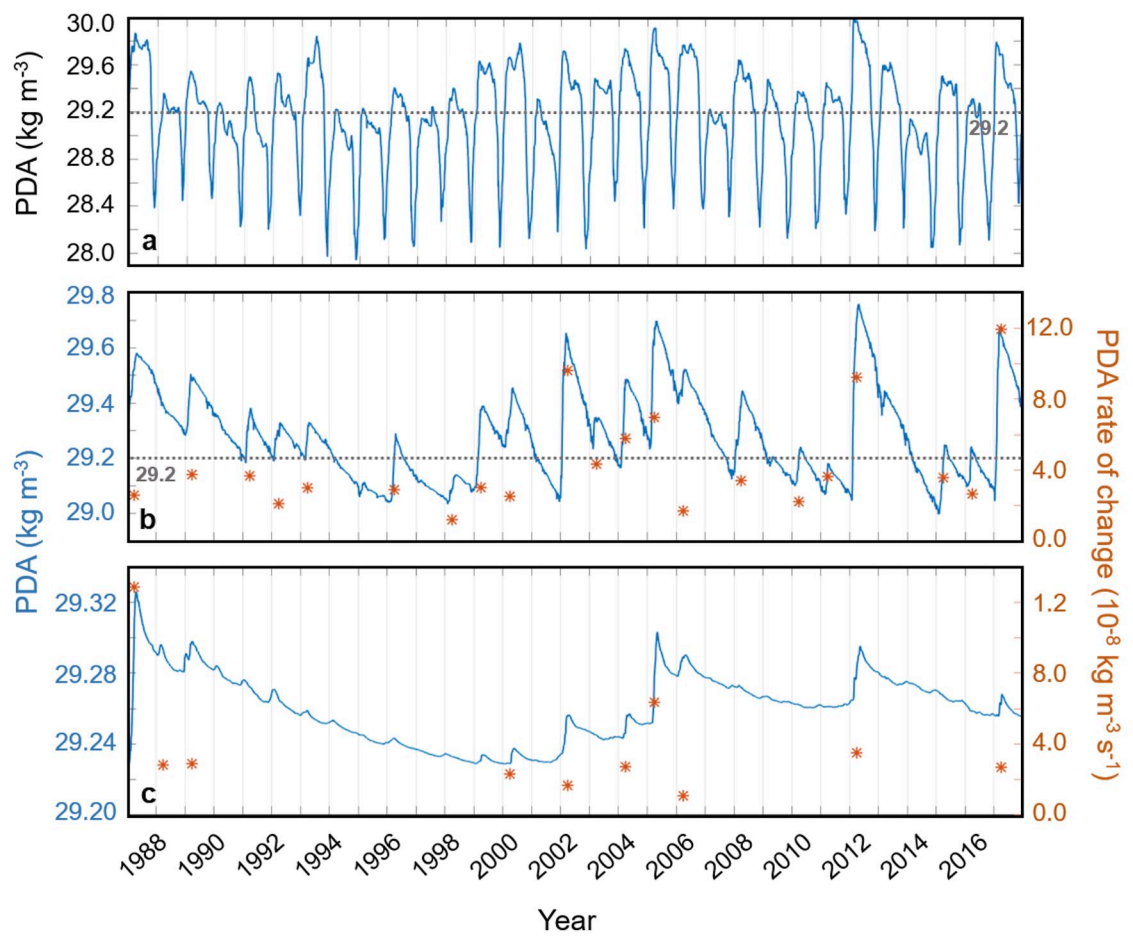


Figure S3.

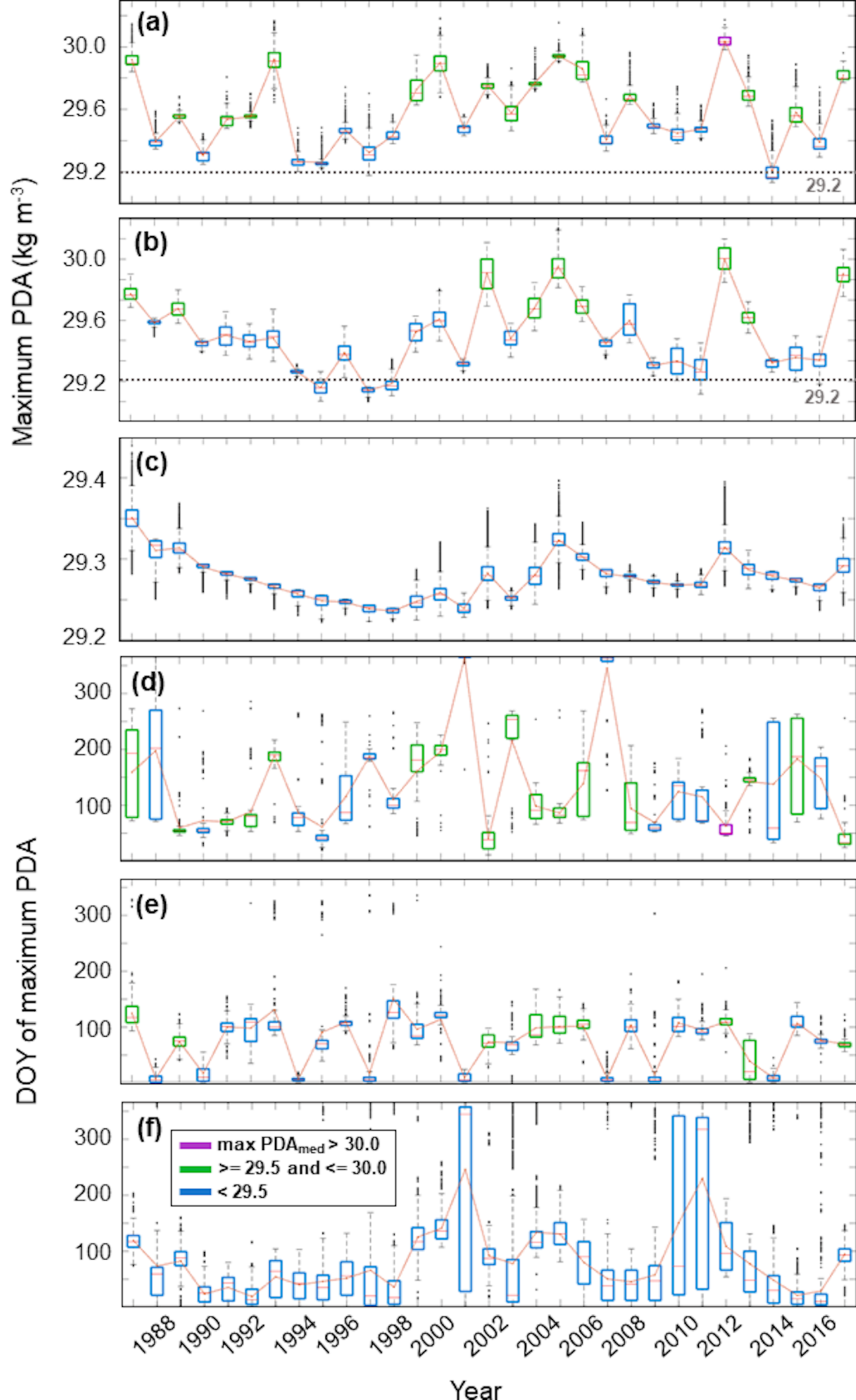


Figure S4.

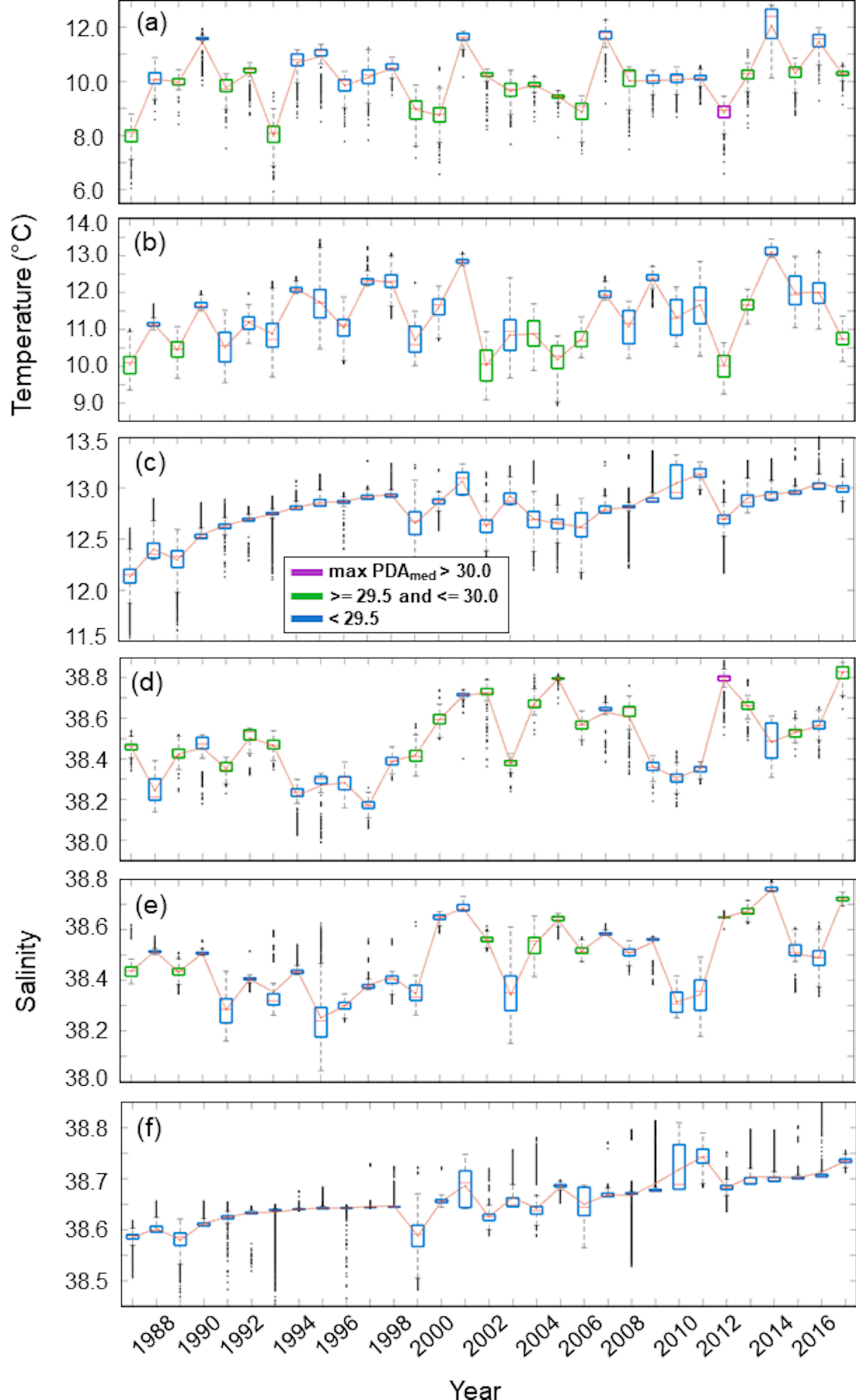
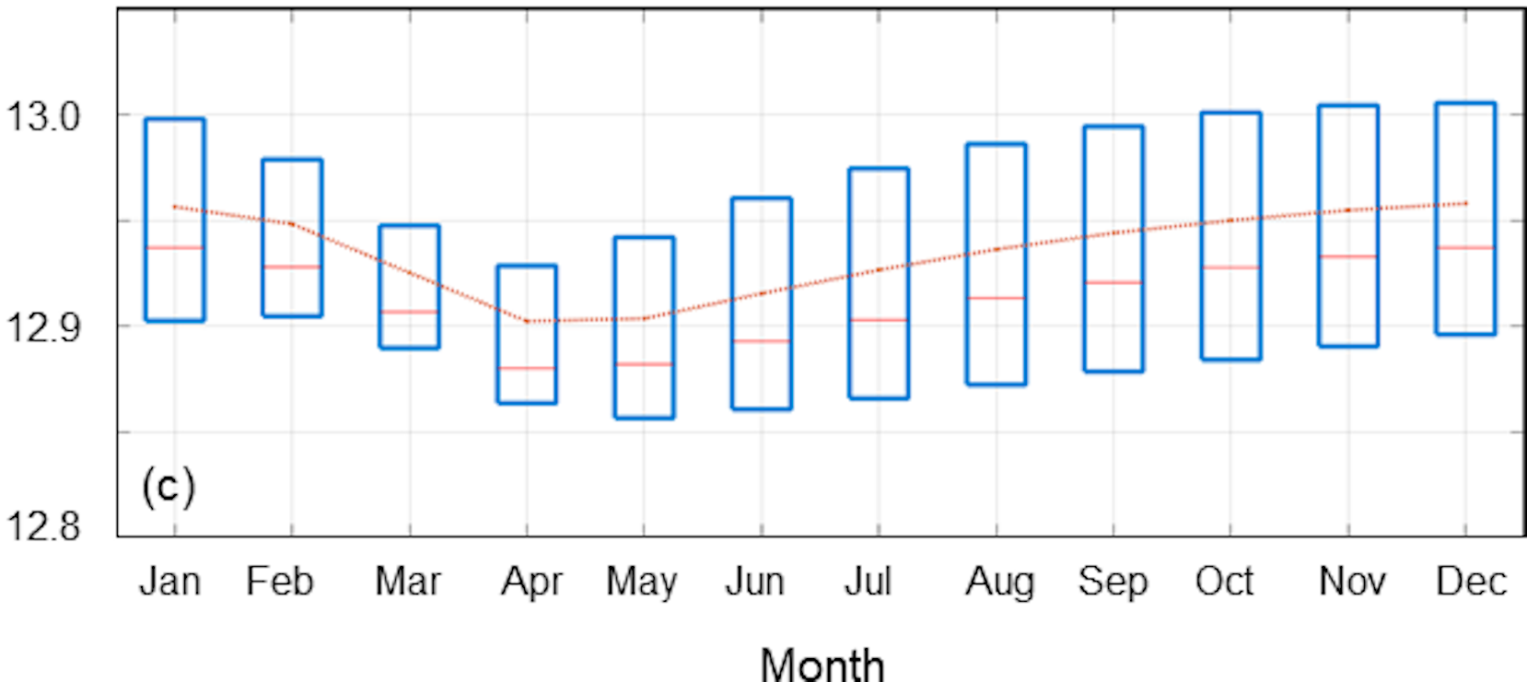
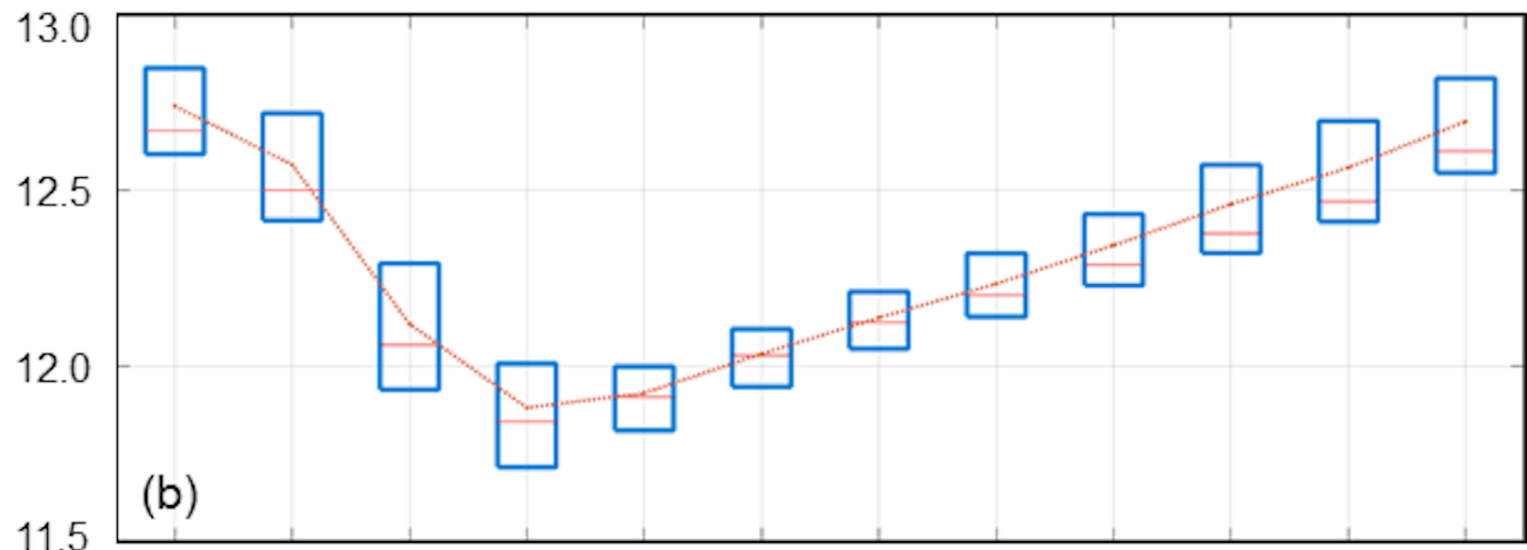
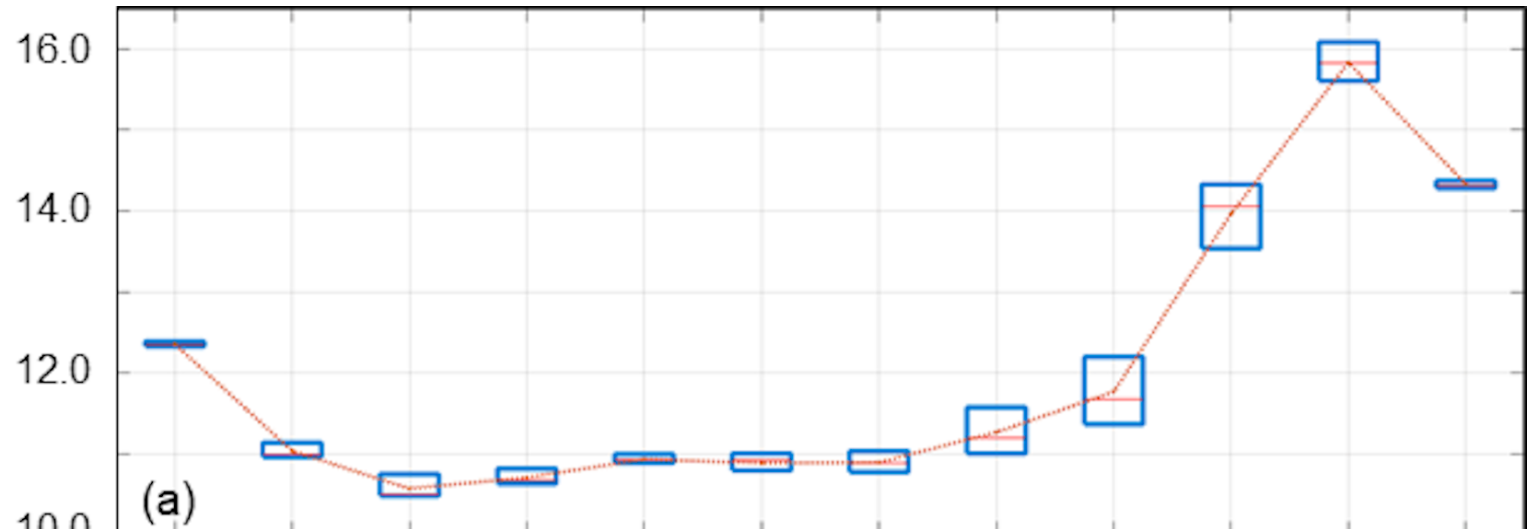


Figure S5.

Temperature ( $^{\circ}\text{C}$ )

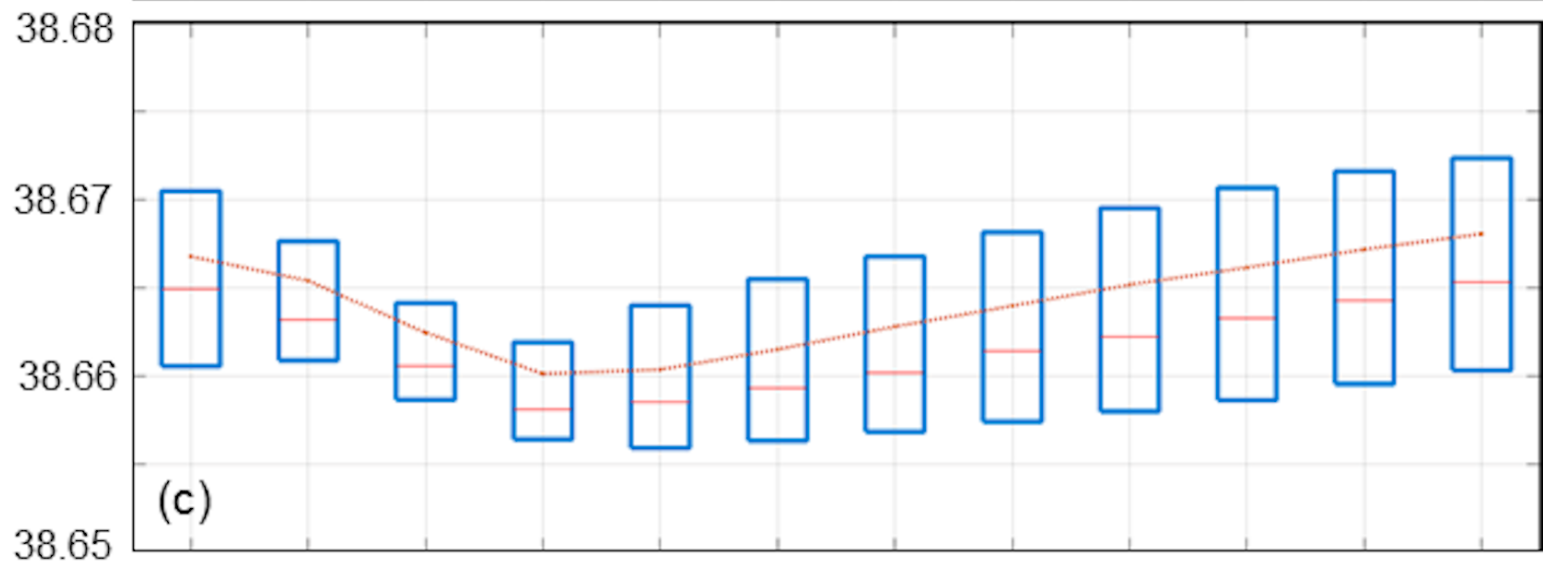
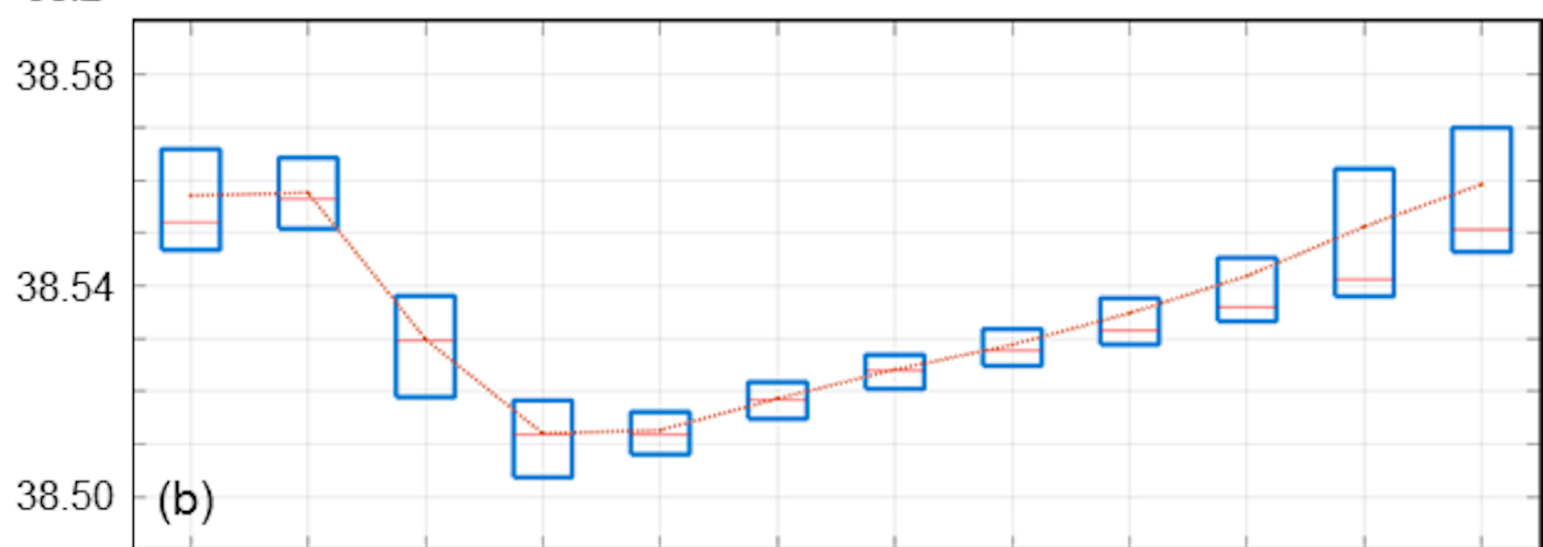
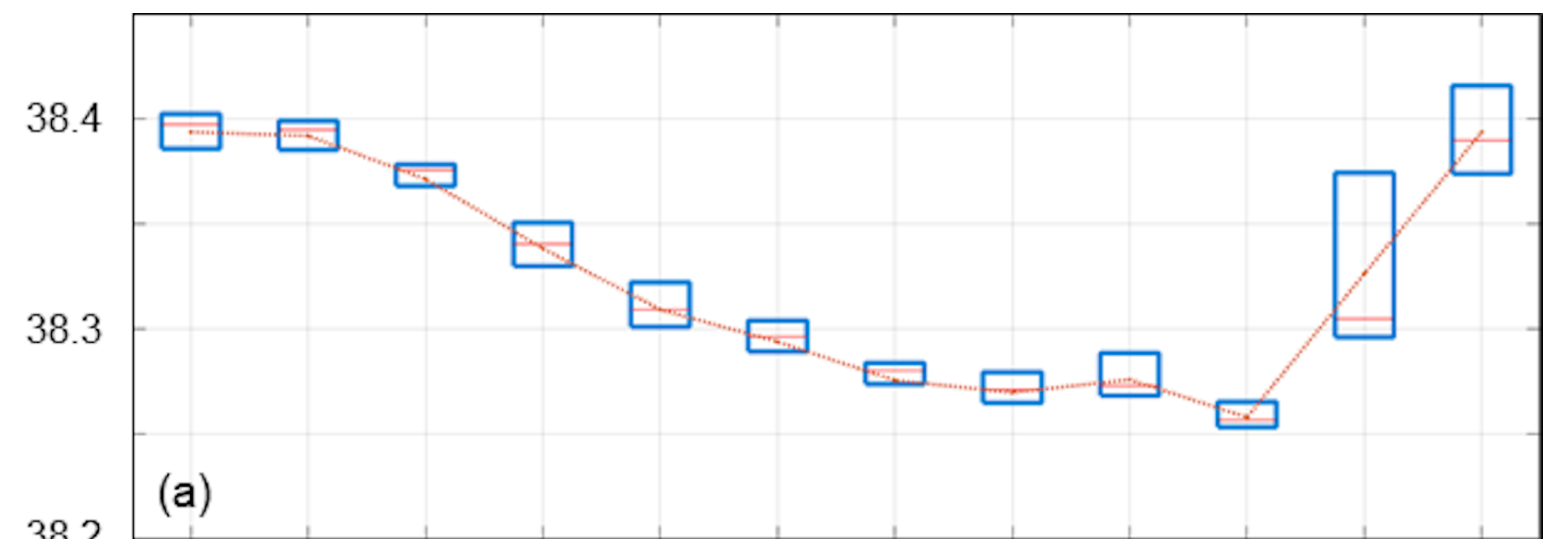


Jan Feb Mar Apr May Jun Jul Aug Sep Oct Nov Dec

Month

Figure S6.

Salinity



Jan Feb Mar Apr May Jun Jul Aug Sep Oct Nov Dec

Month